

Constraints on the Galactic Centre environment from *Gaia* hypervelocity stars II: The evolved population

F. A. Evans¹,^{*} T. Marchetti² and E. M. Rossi¹

¹*Leiden Observatory, Leiden University, PO Box 9513, NL-2300 RA Leiden, the Netherlands*

²*European Southern Observatory, Karl-Schwarzschild-Strasse 2, D-85748 Garching bei München, Germany*

Accepted 2022 September 27. Received 2022 September 20; in original form 2022 May 24

ABSTRACT

A dynamical encounter between a stellar binary and Sgr A* in the Galactic Centre (GC) can tidally separate the binary and eject one member with a velocity beyond the escape speed of the Milky Way. These hypervelocity stars (HVSs) can offer insight into the stellar populations in the GC environment. In a previous work, our simulations showed that the lack of main sequence HVS candidates with precise astrometric uncertainties and radial velocities in current data releases from the *Gaia* space mission places a robust upper limit on the ejection rate of HVSs from the GC of $3 \times 10^{-2} \text{ yr}^{-1}$. We improve this constraint in this work by additionally considering the absence of post-main sequence HVSs in *Gaia* Early Data Release 3 as well as the existence of the HVS candidate S5-HVS1. This evidence offers degenerate joint constraints on the HVS ejection rate and the stellar initial mass function (IMF) in the GC. For a top-heavy GC IMF as suggested by recent works, our modelling motivates an HVS ejection rate of $\eta = 0.7^{+1.5}_{-0.5} \times 10^{-4} \text{ yr}^{-1}$. This preferred ejection rate can be as large as 10^{-2} yr^{-1} for a very top-light IMF and as low as $10^{-4.5} \text{ yr}^{-1}$ if the IMF is extremely top-heavy. Constraints will improve further with future *Gaia* data releases, regardless of how many HVS candidates are found therewithin.

Key words: binaries: general – stars: kinematics and dynamics – Galaxy: centre – Galaxy: nucleus – Galaxy: stellar content.

1 INTRODUCTION

The pursuit of identifying and studying fast-moving Milky Way stars is now entering its second century (Barnard 1916; van Maanen 1917; Oort 1926). With peculiar velocities of tens to hundreds of km s^{-1} , the so-called runaway stars have long been recognized for their potential to provide insight into the dynamical and astrophysical phenomena responsible for accelerating them, particularly the disruption of binaries following a supernova explosion (Blaauw 1961; Boersma 1961; Tauris & Takens 1998; Eldridge, Langer & Tout 2011; Renzo et al. 2019) and ejections following dynamical encounters in young stellar systems (Poveda, Ruiz & Allen 1967; Leonard 1991; Perets & Šubr 2012; Oh & Kroupa 2016).

While very fast ejections from each of the above mechanisms are possible in rare circumstances (Leonard & Duncan 1990; Portegies Zwart 2000; Gvaramadze, Gualandris & Portegies Zwart 2009; Tauris 2015; Evans, Renzo & Rossi 2020), for early-type stars the upper limit on the ejection velocity appears to be $\sim 450 \text{ km s}^{-1}$ (see Irrgang et al. 2019). Alternative mechanisms must therefore be invoked for stars with peculiar velocities above the Galactic escape velocity ($\sim 500 \text{ km s}^{-1}$ at the Solar position; Deason et al. 2019; Koppelman & Helmi 2021; Necib & Lin 2022). Arguably the most attractive option of these alternatives is the Hills (1988) mechanism, in which a stellar binary is disrupted following a dynamical encounter with Sgr A*, the $\sim 4 \times 10^6 M_{\odot}$ supermassive black hole located in the Galactic Centre (GC; Ghez et al. 2008; Genzel, Eisenhauer &

Gillessen 2010). One member of the former binary is ejected as a *hypervelocity star* (HVS) at a characteristic velocity up to and beyond $\sim 1000 \text{ km s}^{-1}$ (Hills 1988; Gould & Quillen 2003; Yu & Tremaine 2003; Bromley et al. 2006; Generozov 2021). On their outward journeys through the Galaxy and beyond to intergalactic space, a sizeable sample of these stars would serve as a valuable dynamical tracer for the Galactic potential out to large distances (Gnedin et al. 2005; Yu & Madau 2007; Kenyon et al. 2008, 2014; Contigiani, Rossi & Marchetti 2019).

This Hills mechanism is also an enticing explanation for the S-star cluster, a population of early-type stars on close, eccentric orbits (Gillessen et al. 2009, 2017) about Sgr A* within the innermost arcsecond ($\sim 0.04 \text{ pc}$) of the Galaxy, where tidal forces from Sgr A* are thought to impede *in-situ* star formation (but see Habibi et al. 2017). The scattering of stellar binaries from the nuclear star cluster (see Launhardt, Zylka & Mezger 2002; Schödel et al. 2014a,b; Neumayer, Seth & Böker 2020) or from substructures within it on to orbits with close periaapses to Sgr A* leads to Hills exchange encounters – one star is ejected as an HVS and its former companion remains bound to Sgr A* as an S-star (Perets, Hopman & Alexander 2007; Madigan, Levin & Hopman 2009; Zhang, Lu & Yu 2013; Madigan et al. 2014; Generozov & Madigan 2020). Since they are GC-born objects located elsewhere on the sky, a sizeable, uncontaminated sample of HVSs with precisely known kinematics would also be useful as a tool to study the stellar environment in the GC (Rossi et al. 2017; Evans, Marchetti & Rossi 2022), where direct observation is complicated by extreme and highly inhomogeneous dust extinction (see Schödel et al. 2014a, for a review).

* E-mail: evans@strw.leidenuniv.nl

After the first serendipitous HVS detections (Brown et al. 2005; Edelmann et al. 2005; Hirsch et al. 2005), several dozen HVS candidates were reported in the decade following (e.g. Brown et al. 2006; Heber et al. 2008; Tillich et al. 2009; Irrgang et al. 2010; Brown, Geller & Kenyon 2012, 2014; Palladino et al. 2014; Zhong et al. 2014). See Brown (2015) for a review on HVSs. Of particular note is S5-HVS1 (Koposov et al. 2020), a $2.35 M_{\odot}$ HVS candidate discovered in the Southern Stellar Stream Spectroscopic Survey (S⁵; Li et al. 2019). In contrast to other HVS candidates, the trajectory of S5-HVS1 unambiguously implies an origin in the GC.

Recently, our knowledge on the kinematics of Milky Way stars both fast and slow has been revolutionized by the European Space Agency’s ongoing *Gaia* mission (Gaia Collaboration 2016a, 2018, 2021a, 2022). With unprecedented astrometric measurements of ~ 2 billion Galactic sources and radial velocity measurements for a subset of \sim tens of millions of cool, bright stars, *Gaia* has demystified the origins of some HVS candidates (Brown et al. 2018; Irrgang, Kreuzer & Heber 2018; Erkal et al. 2019; Kreuzer, Irrgang & Heber 2020) recategorized others as spurious detections and/or bound stars (Boubert et al. 2018, 2019; Marchetti 2021), and discovered new (candidate) stars with extreme velocities (Bromley et al. 2018; Hattori et al. 2018; Shen et al. 2018; Du et al. 2019; Luna, Minniti & Alonso-García 2019; Marchetti, Rossi & Brown 2019; Li et al. 2021; Marchetti 2021). While these unbound star candidates are each fascinating in their own right, it is conspicuous that promising genuine HVS candidates, i.e. unbound stars with precisely known kinematics and trajectories that uncontroversially suggest an origin in the GC, have yet to be unearthed using data solely available in the radial velocity catalogues of *Gaia* Data Release 1, Data Release 2 (DR2) nor Early Data Release 3 (EDR3).

Though somewhat disheartening, Kollmeier et al. (2009, 2010) showed how the absence of confident HVS candidates in a particular survey is in itself a valuable observational result. The Galactic HVS population is directly related to the stellar environment in the GC (Sari, Kobayashi & Rossi 2010; Kobayashi et al. 2012; Rossi, Kobayashi & Sari 2014). If the GC were particularly effective at ejecting HVSs, *Gaia* should be able to see them. An absence of detected HVSs in *Gaia* DR2/EDR3 would then refute models of the inner parsecs of the Galaxy incompatible with this null detection. We investigated this in Evans et al. (2022), hereafter E22. Simulating the ejection of main sequence HVSs from the GC, we showed that the lack of high-confidence HVS candidates in *Gaia* DR2/EDR3 dictates that HVSs must be ejected from the GC at a rate no larger than $\sim 3 \times 10^{-2} \text{ yr}^{-1}$. Forecasting ahead, we showed the HVS populations (or lack thereof) to appear in the then future with the release of *Gaia* Data Release 3 (DR3) and Data Release 4 (DR4) would improve this constraint considerably and would additionally constrain the slope of the stellar initial mass function (IMF) in the GC. We showed as well that while the population of *Gaia*-visible HVSs does depend on the orbital separation and mass ratio distributions among the HVS progenitor binaries, this dependence is too subtle to provide meaningful constraints on these properties given the current paucity of positive detections.

In this work, we expand upon E22 in several ways. We simulate the ejection of HVSs which have evolved off the main sequence, either before or after their ejection from the GC. While post-main sequence HVSs are a minority of Galactic HVSs, they offer a number of advantages in the particular context of the *Gaia* DR2/EDR3 radial velocity catalogues. For the *Gaia* DR2/EDR3 spectroscopic pipeline to assign a validated radial velocity to a source, it must be brighter than the 12th magnitude in the *Gaia* G_{RVS} band (Gaia Collaboration 2018) and it must have an effective temperature in the

range $3500 \text{ K} < T_{\text{eff}} < 6900 \text{ K}$ (Katz et al. 2019). This temperature condition is restrictive for main sequence HVSs, as the hot-end limit corresponds roughly to a stellar mass of $1.5 M_{\odot}$ (Pecaut & Mamajek 2013). A main sequence star of this mass must be less than ~ 1 kpc away to satisfy $G_{\text{RVS}} < 12$. Since HVSs are ejected isotropically from the GC $\simeq 8$ kpc away from Earth, only a slim minority of HVSs are closer than 1 kpc away (E22, c.f. fig. A2). Post-main sequence stars, however, are significantly cooler and intrinsically much brighter than main sequence stars at fixed stellar mass. Stellar evolution models predict that nearly *all* giants and supergiants are cooler than $T_{\text{eff}} = 6900 \text{ K}$. With these cooler temperatures and higher luminosities, post-main sequence HVSs up to ~ 10 kpc away can appear in the *Gaia* DR2/EDR3 radial velocity catalogue. Despite comprising only 8 percent of total Galactic HVSs, the effective observation volume for post-main sequence HVSs is 1000 times larger than for main sequence HVSs. When combined, the more-numerous main sequence HVSs and the easier-to-detect evolved HVSs allow stricter constraints on the GC stellar environment than the main sequence HVSs alone.

To keep focus on *Gaia*, the only existing HVS observational evidence we considered in E22 was the lack of HVS candidates with radial velocities in DR2/EDR3. With the groundwork laid, however, more evidence can be considered. In particular we consider the existence of S5-HVS1 as well. While it has *Gaia* astrometry, S5-HVS1 is neither bright nor cool enough to appear in the *Gaia* DR2/EDR3 radial velocity catalogues. Even so, it remains to date the only uncontroversial HVS candidate. A robust model of the GC stellar environment and the ejection of HVSs must make predictions simultaneously consistent with the lack of HVS candidates in *Gaia* DR2/EDR3 and the existence of S5-HVS1.

In Section 2 of this work we describe our HVS ejection model, in which we eject mock populations of both main sequence and evolved HVSs from the GC, propagate them through the Galaxy and obtain mock observations. In Section 3 we present our results, exploring the population of HVSs at different evolutionary stages we predict to lurk in current and future *Gaia* data releases. We use these predictions to investigate how the lack of HVSs in *Gaia* EDR3 and the existence of S5-HVS1 constrains the GC stellar environment, and show how these constraints will improve with future *Gaia* data releases. In Section 4 we discuss the implications of these results and their caveats, and highlight interesting sub-populations within our mock HVS populations. Finally, we present our conclusions in Section 5.

2 EJECTION MODEL

Our model for the generation, ejection, propagation, and observation of our mock HVS populations is similar to the Monte Carlo (MC) model used in E22. We briefly describe the model and its updates here and refer the reader to E22 (see also Marchetti et al. 2018; Evans et al. 2021) for more detailed information. The model we describe in this section is implemented in the publicly available PYTHON package SPEEDYSTAR.¹

2.1 Generating and ejecting HVSs

In our HVS ejection model, four parameters define the initial conditions of the HVS progenitor binary: the zero-age main sequence (ZAMS) mass of the larger star in the binary (m_p), the mass ratio q

¹<https://github.com/fraserevans/speedystar>

$\equiv m_s/m_p$ between the less-massive secondary (m_s) and primary; a , the orbital semimajor axis of the binary at the moment it is tidally separated; and $\xi \equiv \log_{10}[Z/Z_\odot]$, the total stellar metallicity for both stars in the binary. We draw m_p in the range $[0.1, 100] M_\odot$ assuming a single power-law IMF with slope κ , i.e. $f(m_p) \propto m_p^\kappa$. We assume binary mass ratios are also distributed as a power law with log-slope γ , confined to the range $0.1 \leq q \leq 1$. Orbital semimajor axes are drawn assuming binary orbital periods are distributed as $f(\log P) \propto (\log P)^\pi$, where π is the log-period power law slope. Minimum periods are set following the approximations of Eggleton (1983) to ensure that neither member star of the binary is filling its Roche lobe at the moment of tidal separation. With this minimum period set, interaction between the stars is minimal and each can be assumed to evolve as if it were isolated. Finally, for each system we sample ξ in the range $[-0.25, +0.25]$ assuming a solar metallicity of $Z_\odot = 0.0142$ (Asplund et al. 2009). Stellar metallicities in the GC environment exhibit a significant spread with a slightly super-solar mean (Do et al. 2015; Feldmeier-Krause et al. 2017; Rich et al. 2017; Feldmeier-Krause et al. 2020; Schödel et al. 2020).

There are numerous indications that the IMF in the GC, at least among certain stellar substructures, is top-heavy (e.g. Paumard et al. 2006; Maness et al. 2007; von Fellenberg et al. 2022). We choose $\kappa = -1.7$ as our fiducial power-law IMF slope following Lu et al. (2013), hereafter L13, based on Keck observations of the young stellar population within the innermost half-parsec of the GC. We will also at times highlight a model with a particularly top-heavy IMF in which $\kappa = -0.45$ (Bartko et al. 2010, hereafter B10) and one which follows a canonical Salpeter (1955) (hereafter S55) IMF, i.e. $\kappa = -2.35$. In E22 we showed that the number of high-confidence HVS candidates appearing in current and future *Gaia* data releases is not particularly sensitive to the binary mass ratio distribution log-slope γ and the log-period power-law slope π . We have confirmed that this remains true for evolved HVSSs. When generating mock HVS populations we therefore sample γ and π uniformly in the ranges $[-3, +2]$ and $[-2, +2]$ respectively, capturing the range of values reported in studies of massive binaries in star-forming regions in the Galaxy and the Magellanic Clouds (Sana et al. 2012, 2013; Moe & Stefano 2013; Dunstall et al. 2015; Moe & Di Stefano 2015).

Following the tidal separation of the binary, one star is ejected while the other remains bound to Sgr A*. If the binary approached Sgr A* on a parabolic orbit, the primary and secondary members of the binary are equally likely to be ejected as the HVS (Sari et al. 2010; Kobayashi et al. 2012). We therefore randomly designate one star as the ejected one. It has a stellar mass m_{ej} and its ejection velocity is calculated analytically (Sari et al. 2010; Kobayashi et al. 2012; Rossi et al. 2014):

$$v_{ej} = \sqrt{\frac{2Gm_c}{a}} \left(\frac{M_{\text{SgrA}^*}}{M} \right)^{1/6}, \quad (1)$$

where $M = m_s + m_p = (1 + q)m_p$ is the total mass of the progenitor binary, $m_c = M - m_{ej}$ is the mass of the non-HVS member of the former binary that remains bound to Sgr A*, and $M_{\text{SgrA}^*} = 4 \times 10^6 M_\odot$ (Eisenhauer et al. 2005; Ghez et al. 2008). We assume that stars are ejected from the GC at a constant rate η and that the mass of Sgr A* remains unchanged with time. We choose $\eta = 10^{-4} \text{ yr}^{-1}$ (see Brown 2015) as our fiducial ejection rate.

Our present-day mock ejected star population consist of stars ejected t_{ej} ago that are not yet stellar remnants. We assume that the GC has been ejecting stars without pause since its time of formation, taken here to be shortly after the big bang approximately 13.8 Gyr

ago (Planck Collaboration VI 2020). We assign t_{ej} uniformly:

$$t_{ej} = \epsilon_1 \cdot 13.8 \text{ Gyr}, \quad (2)$$

where $0 < \epsilon_1 < 1$ is a uniform random number. In practice, only HVSSs ejected less than ~ 50 Myr ago will be close enough (and thus bright enough) to be assigned a radial velocity in any current or future *Gaia* data release. We assume both stars in the binary reach ZAMS at the same time. Each star has a maximum lifetime t_{life} , taken here as the elapsed time necessary for a star to evolve from ZAMS to the moment it first becomes a stellar remnant. We assume that at ejection there is no preference for older or younger HVSSs, and therefore we say the age of the binary at ejection $t_{\text{age, ej}}$ is a random fraction ϵ_2 of the maximum total lifetime of the binary:

$$t_{\text{age, ej}} = \epsilon_2 \cdot t_{\text{max}}, \quad (3)$$

where $t_{\text{max}} \equiv \min[t_{\text{life}}(m_c), t_{\text{life}}(m_{ej}), 13.8 \text{ Gyr}]$ to ensure that (i) both stars are non-remnants at the time of ejection, and (ii) the binary is not older than the Universe, as $t_{\text{life}} > 13.8 \text{ Gyr}$ is often true of low-mass stars. We calculate t_{life} for each ejected star using the single stellar evolution SSE algorithms of Hurley, Pols & Tout (2000) as implemented within The Astrophysical Multipurpose Software Environment, or AMUSE² (Portegies Zwart et al. 2009, 2013; Pelupessy et al. 2013; Portegies Zwart & McMillan 2018).

After ejection, the remaining lifetime of the star t_{left} is

$$t_{\text{left}} = t_{\text{life}}(m_{ej}) - t_{\text{age, ej}}. \quad (4)$$

We remove stars for whom $t_{ej} > t_{\text{left}}$, i.e. stars which are remnants at the present day. The flight time of each surviving mock ejected star is then

$$t_{\text{flight}} = t_{ej} \quad (5)$$

and its current age is

$$t_{\text{age, 0}} = t_{\text{age, ej}} + t_{\text{flight}}. \quad (6)$$

2.2 Orbital integration

We assume that the Hills mechanism ejects stars isotropically away from Sgr A*. We therefore eject HVSSs in random directions, initializing them on random points on the surface of the Sgr A* sphere of influence 3 pc in radius (Genzel et al. 2010) with initial velocities pointing radially away from the GC. We then propagate the stars through the Milky Way using the Galactic potentials of McMillan (2017), who fit a many-component potential to various kinematic data using a Monte Carlo Markov Chain (MCMC) method. For each realization in which we eject stars from the GC, we draw a Solar position and velocity from among the McMillan (2017) MC chain (P. McMillan, private communication) as well as a Galactic potential. Using a fifth-order Dormand-Prince integrator (Dormand & Prince 1980) and a timestep of 0.1 Myr, we integrate ejected star trajectories through this potential using the PYTHON package GALPY³ (Bovy 2015).

2.3 Mock photometric observations

We determine the current luminosity, effective temperature, radius, and surface gravity for each ejected star using the SSE models implemented within AMUSE. We also identify each star's current

²<https://amuse.readthedocs.io/en/latest/index.html>

³<https://github.com/jobovy/galpy>

evolutionary stage (e.g. main sequence, red giant, core helium-burning) adopting the conventions of Hurley et al. (2000) to designate stages. Next, we calculate the visual extinction A_V at each star's distance and sky position using the MWDUST⁴ 3D Galactic dust map (Bovy et al. 2016) assuming a Cardelli, Clayton & Mathis (1989) reddening law with $R_V = 3.1$. From each star's temperature, surface gravity and visual extinction, we obtain mock photometric observations using the MESA Isochrone and Stellar Tracks, or MIST (Choi et al. 2016; Dotter 2016) model grids.⁵ We interpolate the appropriate bolometric correction tables to determine each star's apparent magnitude in the *Gaia* EDR3 G and G_{RP} bands⁶ (Riello et al. 2021) as well as the Johnson-Cousins V and I_c bands (Bessell 1990). The apparent magnitude in the *Gaia* G_{RVS} band can then be computed from the G , V , and I_c magnitudes using the polynomial fits in Jordi et al. (2010) (table 3). To select stars which would appear in the S^5 survey, we determine each star's apparent magnitude in the Dark Energy Camera (DECam) g and r filters (Abbott et al. 2018) as well.

2.4 Identifying *Gaia*-visible HVSs

With apparent magnitudes computed, we next identify which stars would appear as promising HVS candidates in various *Gaia* data releases. As in E22, these stars must satisfy three criteria:

- (i) They must satisfy the apparent magnitude and effective temperature conditions (described below) to appear in the radial velocity catalogue of a given data release.
- (ii) Their mock relative parallax uncertainties must be <20 per cent, otherwise distance estimation becomes non-trivial (see Bailer-Jones 2015).
- (iii) When comparing its Galactocentric velocity to the Galactic escape velocity at its position according to the best-fitting potential of McMillan (2017), it must have an >80 per cent chance of being unbound to the Galaxy when sampling over its astrometric and radial velocity uncertainties.

These above cuts match closely those used to search for HVS candidates in *Gaia* DR2 (Marchetti et al. 2019) and EDR3 (Marchetti 2021). For concision, when we use the terms '*Gaia* DR2/(E)DR3/DR4' we are referring exclusively to the subsets of these data releases with measured radial velocities, and by the term 'HVS' we refer only to those stars which satisfy these criteria.

The faint-end magnitude limit for the *Gaia* DR2 radial velocity catalogue is $G \simeq 12$, though the precise faint-end limit varies on the sky due to the scanning pattern of the *Gaia* satellite itself and due to stellar crowding in source-dense regions such as the GC and Large Magellanic Cloud (see Boubert & Everall 2020; Boubert, Everall & Holl 2020). To more realistically account for these observational realities, we use the *Gaia* DR2 spectroscopic selection function as estimated by Everall & Boubert (2022).⁷ The selection function assigns each star has a probability p of appearing in the *Gaia* DR2 radial velocity catalogue depending on its sky position, brightness, and colour. We classify an HVS as 'DR2-detectable' if a uniform random number $0 < \epsilon < 1$ satisfies $\epsilon < p$. The *Gaia* DR2 spectroscopic pipeline from providing validated radial velocities only for sources with effective temperature ranges in

the range $3500 \text{ K} \leq T_{\text{eff}} \leq 6900 \text{ K}$ (Katz et al. 2019). Mock ejected stars with effective temperatures outside this range are removed from our *Gaia* DR2-detectable sample.

We estimate the *Gaia* DR2 astrometric uncertainties for each star using the DR2 astrometric spread function of Everall et al. (2021).⁸ The astrometric spread function computes the full 5D covariance matrix for each source, providing uncertainties and correlations among the position, parallax, and proper motion. We estimate radial velocity errors for each star based on its V -band magnitude and spectral type using the PYTHON package PyGaia,⁹ and assume for all stars that the radial velocity uncertainties are uncorrelated to the astrometric uncertainties.

We follow a similar procedure to identify high-confidence mock HVS candidates appearing in *Gaia* Early Data Release 3. *Gaia* EDR3 parallax uncertainties are improved by 30 per cent relative to DR2, and proper motion uncertainties improve by a factor of 2 (*Gaia* Collaboration 2021b). EDR3 however, does not provide new or updated radial velocities. *Gaia* DR2 radial velocity measurements have been simply ported to their EDR3 counterparts. We once again use the DR2 spectroscopic selection function of Everall & Boubert (2022) to select stars appearing in this catalogue, the DR3 astrometric spread function of Everall et al. (2021) to assign astrometric uncertainties and PyGaia to assign radial velocity uncertainties.

The full *Gaia* DR3, released 2022 June 13, contains the EDR3 astrometric solutions as well as radial velocity measurements¹⁰ for ~ 33 million sources brighter than $G_{RVS} \simeq 14$ in the effective temperature range [3500 K, 6900 K] (Katz et al. 2019). Improvements in the *Gaia* spectroscopic pipeline¹¹ additionally allow validated radial velocity measurements for $7000 \text{ K} < T_{\text{eff}} < 14500 \text{ K}$ sources to a depth of $G_{RVS} \lesssim 12$. We use these same criteria to select stars detectable in DR3, since more detailed information about the DR3 spectroscopic selection function is not yet available. The DR3 astrometric spread function of Everall & Boubert (2022) and PyGaia are once again used to assign astrometric and radial velocity uncertainties, respectively.

Finally, we identify stars visible in the fourth and (nominally) final *Gaia* data release. Radial velocities will be available for sources cooler than 6900 K and brighter than the $G_{RVS} = 16.2$ mag limiting magnitude of the *Gaia* radial velocity spectrometer (Cropper et al. 2018; Katz et al. 2019). For hotter stars, we make the assumption that validated radial velocities will be available for sources brighter than $G_{RVS} = 14$. We use the astrometric covariance matrix as computed using the Everall et al. (2021) astrometric spread function to estimate the DR4 astrometric covariance matrix. We scale down the diagonal elements of the matrix (corresponding to the astrometric errors) according to the predicted *Gaia* performance – relative to DR3, parallax precisions in DR4 will improve by ~ 33 per cent and proper motion precisions by ~ 80 per cent.¹² We assume that off-diagonal elements, corresponding to the correlations between the astrometric errors, remain unchanged from their DR3 estimations.

In Fig. 1 we illustrate how restrictive our cuts are. After propagation, the left-hand panel shows 68 per cent and 95 per cent density

⁴<https://github.com/jobovy/mwdust>

⁵<https://waps.cfa.harvard.edu/MIST/>

⁶<https://www.cosmos.esa.int/web/gaia/edr3-passbands>

⁷see <https://github.com/gaiaverse/selectionfunctions>

⁸see <https://github.com/gaiaverse/scanninglaw>

⁹<https://github.com/agabrown/PyGaia>

¹⁰This work was initially submitted for publication prior to the release of *Gaia* DR3. In Marchetti, Evans & Rossi (2022) we search for HVS candidates within DR3 and use the methodology of this work to infer updated constraints on the GC environment.

¹¹see <https://www.cosmos.esa.int/web/gaia/dr3>

¹²<https://www.cosmos.esa.int/web/gaia/science-performance>, see also Brown (2019).

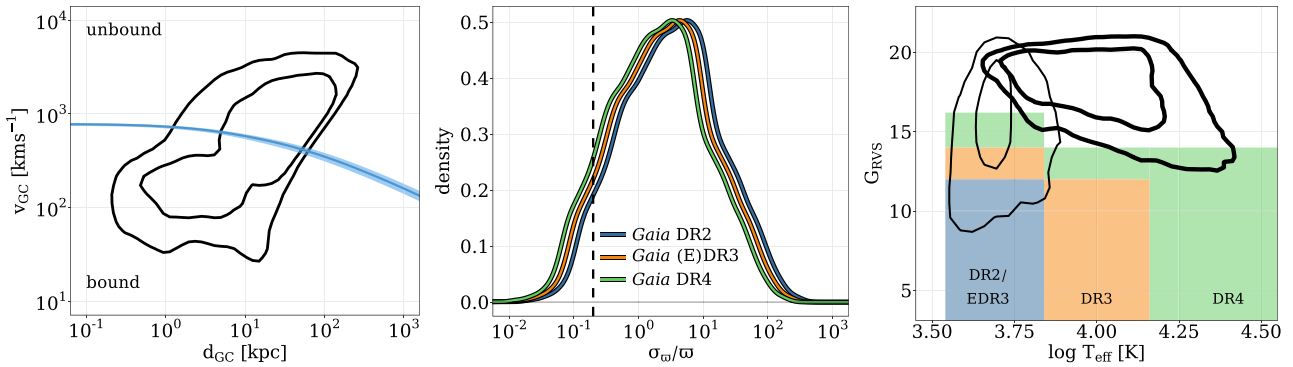


Figure 1. Left-hand panel: 1σ and 2σ contours of the distribution of Hills mechanism-ejected stars in Galactocentric velocity versus distance. The blue curve and shaded region shows the median $\pm 1\sigma$ spread of the escape velocity to infinity from each Galactocentric distance in the McMillan (2017) family of Galactic potentials. Centre: The distribution of the relative *Gaia* parallax uncertainty σ_π/π for mock ejected stars. The blue curve shows *Gaia* DR2 uncertainties and the orange and green curves show predicted (E)DR3 and DR4 performance, respectively. The vertical dashed line shows $\sigma_\pi/\pi = 0.2$. Right-hand panel: Stars must lie in the shaded regions of G_{RVS} versus T_{eff} to be assigned a validated radial velocity in *Gaia* DR2, (E)DR3, and DR4. The thick lines show the 1σ and 2σ density contours for the distribution of main sequence ejected stars in this space. The thin lines show the distribution of post-main sequence stars. In all three panels, only $t_{\text{flight}} \leq 100$ Myr stars brighter than $G = 20.7$ stars are shown.

contours of Galactocentric distances and velocities for stars ejected from the GC in our fiducial model. The escape velocity curve from the best-fitting potential of McMillan (2017) and 1σ scatter is shown with the blue line. To keep focus only on stars with a non-negligible chance of being detected by *Gaia*, we show only stars ejected less than 100 Myr ago that are bright enough to appear in the *Gaia* source catalogue, i.e. brighter than the 20.7th magnitude in the *Gaia* G band (Gaia Collaboration 2016b). Among stars ejected from the GC, there are two distinct populations: a population of stars which remain bound within the inner ~ 10 kpc of the Galaxy with velocities of tens to hundreds of km s^{-1} , and a population unbound to the Galaxy extending to large distances with velocities of $\gtrsim 1000 \text{ km s}^{-1}$. Less than half of ejected stars are unbound to the Galaxy. While valuable information about the Galactic potential and the GC stellar environment is also encoded in stars that are ejected at large-but-not-unbound velocities, unbound stars are easier to identify as promising HVS candidates¹³ and their origins are less ambiguous – they are the focus of this paper. In the centre panel we show how the relative *Gaia* parallax error σ_π/π for our mock HVS populations improves with each *Gaia* data release. The dashed vertical line shows our parallax error cut at $\sigma_\pi/\pi = 0.2$. Only 6 per cent, 8 per cent, and 11 per cent of HVSs will satisfy $\sigma_\pi/\pi < 0.2$ in *Gaia* DR2, (E)DR3 and DR4, respectively. The majority of ejected HVSs will have a relative parallax error $\gg 1$. In the right-hand panel, the shaded regions show the effective temperature and (approximate) G_{RVS} limits of the *Gaia* DR2/EDR3, DR3, and DR4 radial velocity catalogues. In this space, we show the 68 per cent and 95 per cent density contours for the distributions of main sequence (thick lines) and post-main sequence (thin lines) ejected star populations separately. Overall, main sequence HVSs in the *Gaia* source catalogue are too dim and too hot to appear in *Gaia* DR2/EDR3 and DR3, but an appreciable population may be found in DR4 (see also E22). Evolved HVSs fare much better, however. Although they constitute only ~ 8 per cent of total ejected HVSs, a large fraction are sufficiently cool and bright to be assigned radial velocities in *Gaia* DR2/(E)DR3/DR4 in principle.

¹³A proviso: Brown et al. (2007) had success finding *bound* HVS candidates by searching for early-type stars at high Galactic latitudes and large heliocentric distances $d \gtrsim 10$ kpc.

3 RESULTS

3.1 The evolved HVS population

Having explored solely the main sequence HVS population in E22, here we first describe the number of high-confidence HVSs of all evolutionary stages we predict to appear in current and future *Gaia* data releases.

We showed in E22 that the number of HVSs appearing in *Gaia* depends most critically on the assumed IMF slope κ and the HVS ejection rate η . In Fig. 2 we show how the number of HVSs depends on κ in each of *Gaia* DR2, EDR3, DR3, and DR4. We split HVSs into main sequence (MS), subgiant branch or Hertzsprung gap (HG), red giant branch (RGB), and core helium-burning (CHeB) phases. The dotted vertical line shows our fiducial assumption for κ , and the shaded region shows a ± 0.2 uncertainty applied (L13). These are estimates for our fiducial HVS ejection rate of 10^{-4} yr^{-1} – they can be scaled linearly up or down for other ejection rates (c.f. E22, fig. 2) since we assume a constant ejection rate. At this ejection rate, less than one HVS in total is expected in *Gaia* DR2 unless the IMF of HVS progenitor binaries is very top-heavy. Core helium-burning stars are the most likely to appear in this data release, while main sequence, Hertzsprung gap, and red giant branch HVSs are all quite rare and more or less equally likely. For *Gaia* EDR3, ≥ 1 evolved HVSs are expected to appear in this survey if the GC IMF is more top-heavy than our fiducial assumption. Given that no HVS has yet been detected in EDR3, this fact can already place some meaningful constraints on the GC stellar environment. Once again, if HVSs were likely to lurk in this data release, they would most likely be core helium-burning.

Looking ahead to subsequent releases, $1.1^{+1.5}_{-0.9}$ HVS are expected in *Gaia* DR3 given our fiducial assumptions, most likely a core helium-burning HVS. If the IMF of HVS progenitors were to be particularly top-heavy, several core-helium burning would be expected and the probability of detecting a main sequence HVS becomes non-insignificant.

Finally for DR4, we predict $10.9^{+4.8}_{-4.2}$ HVSs for our fiducial model. Unlike earlier data releases, the main sequence HVS population will outnumber evolved ones. Of the $1.4^{+1.6}_{-0.7}$ evolved stars we expect to appear in this data release in our fiducial model, $1.3^{+1.7}_{-0.8}$ will be horizontal branch stars with typical masses of $\sim 5 M_\odot$. Unless the

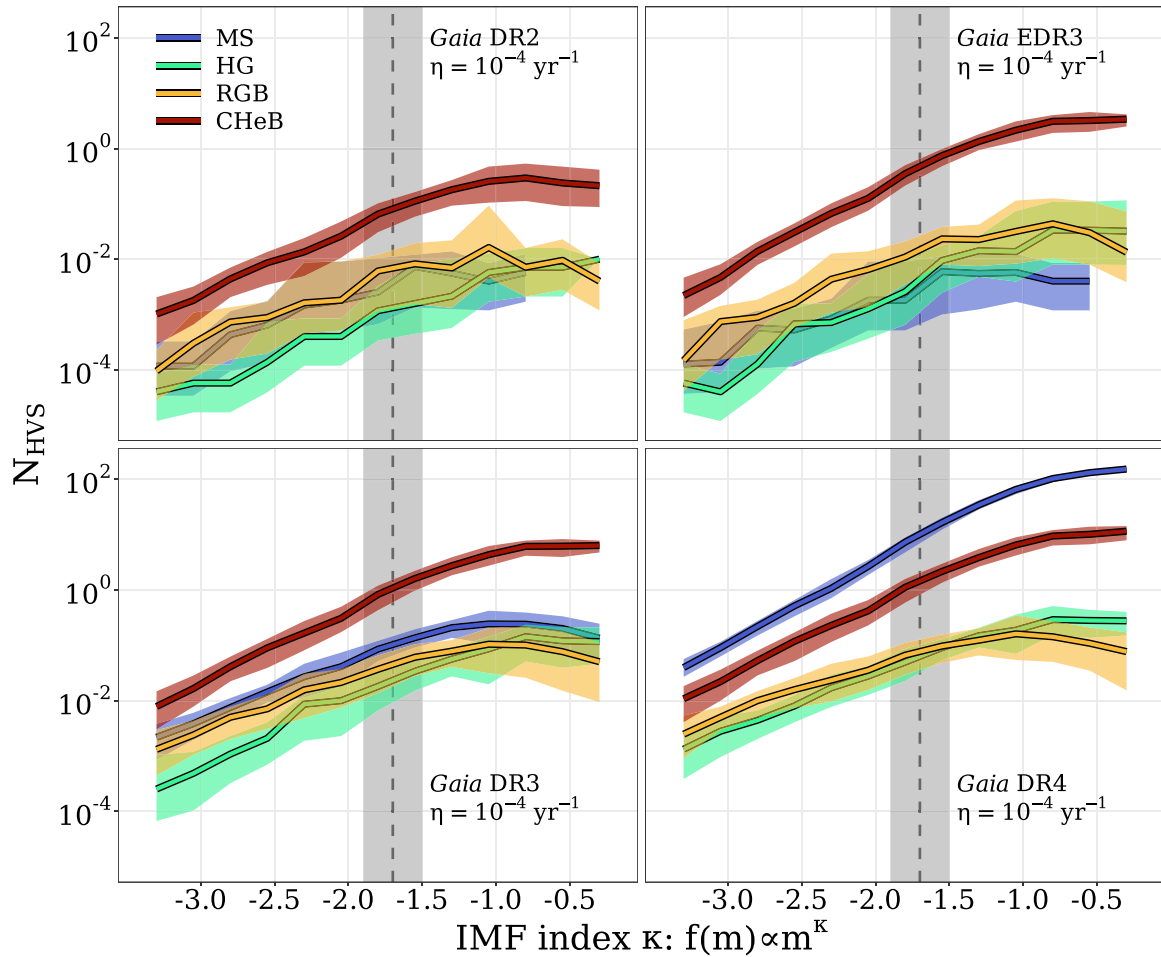


Figure 2. The number N_{HVS} of high-confidence detectable HVSs in the radial velocity catalogues of *Gaia* DR2, EDR3, DR3, and DR4 (clockwise from top-left) plotted against the HVS progenitor IMF index κ for a fixed HVS ejection rate of 10^{-4} yr^{-1} . HVS populations are split into main sequence (MS; blue), Hertzsprung gap/subgiant branch (HG; green), red giant branch (RGB; gold) and core helium-burning (CHeB; red) populations. The shaded regions span the 16th to 84th percentiles over 5000 iterations. The vertical dashed line and shaded region show $\kappa = -1.7 \pm 0.2$ (L13).

IMF is quite top-heavy or the HVS ejection rate quite high, we expect fewer than one hypervelocity Hertzsprung gap or red giant star to appear in DR4. It may seem counterintuitive that predictions for Hertzsprung gap and red giant branch stars are similar throughout Fig. 2 when the Hertzsprung gap is known to be a short phase of evolution. It is helpful to note, however, that 96 per cent of detectable HVSs are more massive than $\sim 2 M_{\odot}$, for whom the red giant branch phase is quite short since their helium core is non-degenerate when it reaches the base of the red giant branch.

When the HVS ejection rate is left as a free parameter, we show with white contour lines in Fig. 3 how of the number $N_{\text{HVS, evolved}}$ of post-main sequence HVSs changes in the $\kappa - \eta$ space for each different *Gaia* data release. The colourscales indicate the 1σ scatter of $N_{\text{HVS, evolved}}$ over 5000 iterations smoothed over the grid. The black-and-white diamonds indicate our fiducial $\kappa = -1.7$ (L13) and $\eta = 10^{-4} \text{ yr}^{-1}$, as well as models with $\kappa = -2.35$ (S55) and $\kappa = -0.45$ (B10) for comparison. Similar plots for the main sequence HVS population can be found in E22, c.f. Fig. 4. There are regions of $\kappa - \eta$ space that predict at least \sim tens or \sim hundreds of high-confidence evolved HVS in *Gaia* DR2 and EDR3. This, however, would be in contradiction to the apparent complete absence of these objects in these data releases. For particularly top-heavy IMFs and reasonably high ejection rates, \sim hundreds of evolved HVSs could be found. DR4

will only grow the evolved HVS population by a modest amount. This is in stark contrast to the main sequence population, which can increase in size by more than two orders of magnitude from DR3 to DR4. In Section 4.3 we discuss interesting hypervelocity subpopulations in greater detail.

Given reasonable (if optimistic) assumptions, the *Gaia* DR3 and DR4 HVS populations could conceivably be large enough to obtain useful summary statistics. To examine these potential populations in greater detail, in Fig. 4 we show how to populate the Hertzsprung–Russell diagram stacked over 5000 iterations with our fiducial κ . In DR3, main sequence HVSs up to $\sim 6 M_{\odot}$ will in principle be present. Detectable core helium-burning stars in this data release would most likely be $m \simeq 2 - 3 M_{\odot}$ stars in the red clump as well as core helium-burning stars during the entirety of a blue loop phase. These same post-main sequence populations will be detectable in DR4, as well as a sizeable main sequence HVS population with a typical mass of $\sim 8 M_{\odot}$.

3.2 Constraining the GC IMF and ejection rate

In E22 we used the absence of main sequence HVSs in *Gaia* DR2 and EDR3 to place constraints on the IMF in the GC and the HVS ejection rate. We showed that unless the IMF among the primaries

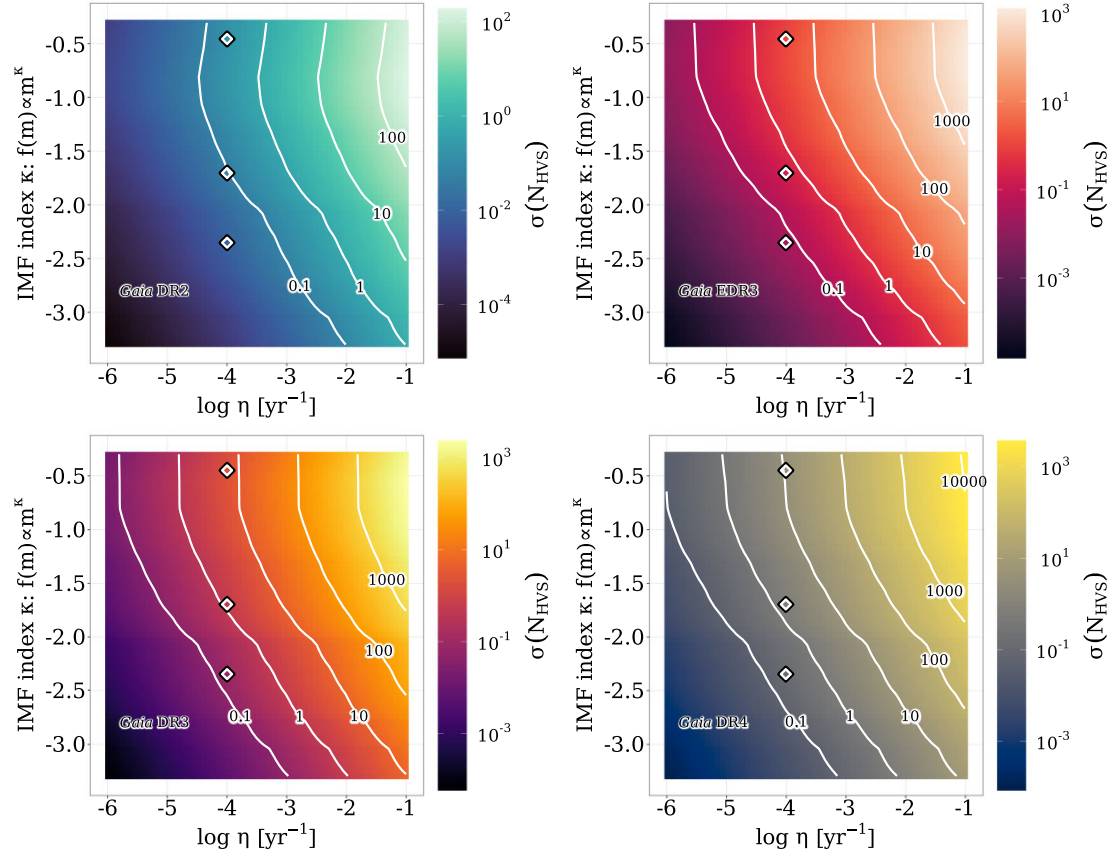


Figure 3. Contour lines show how the numbers $N_{\text{HVS, evolved}}$ of evolved HVs in *Gaia* DR2 (top left-hand panel), EDR3 (top right-hand panel), DR3 (bottom left-hand panel), and DR4 (bottom right-hand panel) change in the 2D parameter space of the IMF power law index κ and the HVS ejection rate η , averaged over 5000 realizations and smoothed over the grid. The colourbar shows how the 1σ scatter of $N_{\text{HVS, evolved}}$ changes in this space. The black-and-white diamonds indicate our fiducial ejection rate of $\eta = 10^{-4} \text{ yr}^{-1}$ and fiducial $\kappa = -1.7$ (L13), as well as $\kappa = -2.35$ (S55) and $\kappa = -0.45$ (B10).

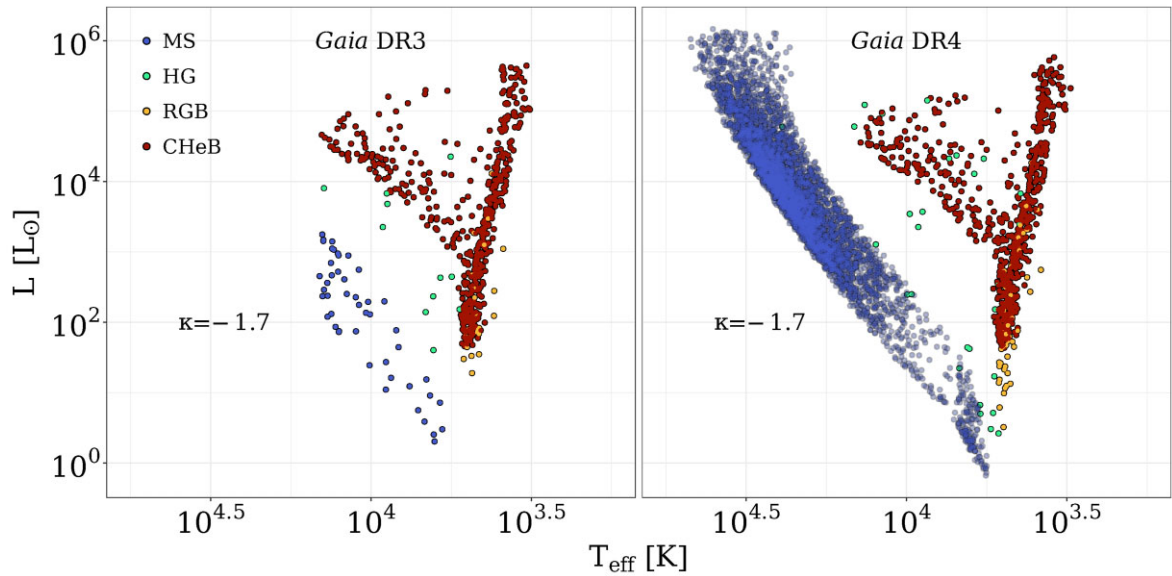


Figure 4. Hertzsprung–Russell diagram for high-confidence detectable HVs in the radial velocity catalogues of *Gaia* DR3 (left-hand panel) and DR4 (right-hand panel) for a fixed IMF slope ($\kappa = -1.7$). Populations are coloured by evolutionary stage as in Fig. 6. Results are shown stacked over 500 iterations. Main sequence HVs in DR4 are plotted with semitransparency to better show the distribution.

of HVS progenitor binaries is extremely top-light ($\kappa \lesssim -3$), ejection rates in excess of $3 \times 10^{-2} \text{ yr}^{-1}$ are excluded at 1σ confidence. With our analysis of evolved HVSs here, we can improve these constraints considerably. In addition, we compute constraints in a more sophisticated way using a Bayesian inference approach. This allows us to use prior information on κ and η and other observational evidence about Milky Way HVSs to strengthen constraints. We compute the posterior probabilities

$$p(\theta|D) = \frac{\mathcal{L}(D|\theta)p(\theta)}{p(D)}, \quad (7)$$

where D is the observed HVS data, $\theta \equiv (\kappa, \eta)$ are model parameters for the IMF index and HVS ejection rate in the GC environment, $\mathcal{L}(D|\theta)$ is the likelihood of observing the data given the particular model, $p(\theta)$ accounts for prior knowledge on the model parameters, and $p(D)$ is a normalizing constant. The combination of these yields the posterior probability for the model parameters $p(\theta|D)$.

In the subsections below we outline the existing data we consider, the priors we consider, and the resulting posterior constraints on κ and η .

3.2.1 The data

A key observation we consider is the lack of unbound HVS candidates with precise astrometry in the radial velocity catalogues of *Gaia* DR2 (Marchetti et al. 2019) and EDR3 (Marchetti 2021), and our selection criteria outlined in Section 2 mirrors quality cuts used in these works. While this places competitive constraints on the GC stellar environment by itself, we can improve constraints further by considering the HVS candidate S5-HVS1 (Koposov et al. 2020), a $\sim 2.35 M_{\odot}$ star with an apparent magnitude of 16.0 in the *Gaia* G band, a breakneck Galactocentric velocity of $v_{\text{ej}} \simeq 1750 \text{ km s}^{-1}$, and a relatively short flight time from the GC of $t_{\text{flight}} \simeq 4.8 \text{ Myr}$. It was identified in a subsurvey of the S^5 survey (Li et al. 2019), which as of 2019 June has covered $\sim 345 \text{ deg}^2$ with 115 fields observed with the Anglo-Australian Telescope (AAT). It can be stated with confidence that S5-HVS1 is the only HVS within the S^5 catalogue – by identifying S5-HVS1 analogues from our mock populations of HVSs, we can determine which models are consistent with S5-HVS1. To identify S5-HVS1 analogues, we roughly reproduce the S^5 selection criteria by taking HVSs within the S^5 footprint (see Li et al. 2019, table 2) which have mock *Gaia* parallaxes satisfying $\varpi < 3\sigma_{\varpi} + 0.2$, mock DECam photometry satisfying $15 < g < 19.5$ and $-0.4 < (g - r) < +0.1$. Since only stars with radial velocities larger than 800 km s^{-1} were selected for further inspection (Koposov et al. 2020), we apply this criterion as well.

3.2.2 The priors

We consider two sets of priors on the IMF index in the GC κ and the HVS ejection rate η ; one set in which we assume uniform priors across the $\kappa - \eta$ range we explore, and one more restrictive set which considers modern determinations of these parameters.

For the set of restrictive priors, we assume κ is normally distributed with a mean at $\kappa = -1.7$ and a standard deviation of 0.2, following from L13 who simultaneously fit several properties of the young stellar cluster in the inner 0.5 pc of the Galaxy. They compare the *Keck* K' -band luminosity function of young stars in the GC (Do et al. 2013) to mock observations of synthetic star clusters to determine this IMF slope via a Bayesian inference approach. While not quite as top-heavy as other IMF determinations near the centre of the Galaxy

(e.g. Bartko et al. 2010), this is but another indication that the initial mass function, at least among young stellar structures in the GC, is at least modestly top-heavy (see E22, Section 3 and references therein).

A recent, robust determination of the HVS ejection rate η with associated uncertainties does not yet exist. However, reasonable estimates from theoretical modelling (Hills 1988; Yu & Tremaine 2003), detailed simulations (Zhang et al. 2013), and calibration to known HVS candidates (Bromley et al. 2012; Brown et al. 2014; Marchetti et al. 2018) and to rates of tidal disruption events (see Bromley et al. 2012; Brown et al. 2015; Stone et al. 2020) support an ejection rate in the range $10^{-5} \text{ yr}^{-1} - 10^{-3} \text{ yr}^{-1}$. For our set of restrictive priors we therefore assume a prior of the form

$$p(\log \eta) \propto \tanh[\ell(\log \eta - (-5) - \pi/\ell)] - \tanh[\ell(\log \eta - (-3) + \pi/\ell)], \quad (8)$$

where $\ell = 8$ is a smoothing parameter, such that the prior probability is uniform between 10^{-5} and 10^{-3} yr^{-1} and quickly and smoothly drops to zero outside this range. We assume the priors on κ and η are entirely uncorrelated, i.e. $p(\kappa, \eta) = p(\kappa)p(\eta)$.

3.2.3 The likelihood

The likelihoods $\mathcal{L}(D|\theta)$ are computed with an MC approach. For each (κ, η) combination in our model grid, $\mathcal{L}(D|\theta)$ is the probability computed over 5000 repeated MC realizations that the model simultaneously satisfies zero HVSs being found in *Gaia* EDR3 and the existence one (and only one) S5-HVS1 analogue, where S5-HVS1 analogues are selected as described above. These outcomes are not independent – if a particular realization results in many EDR3-detectable HVSs, it is likely to produce many S5-HVS1 analogues as well.

3.2.4 The posteriors

In Fig. 5 we show the outcome of our Bayesian modelling (equation 7), broken up to show how each consideration of the data and priors impact the resulting posterior distributions. In the top left-hand panel, the colourbar shows the posterior probabilities for (κ, η) combinations if only the lack of credible HVS candidates in the *Gaia* EDR3 radial velocity catalogue is considered and we assume uniform priors. The thin and thick red contours highlight the 68 per cent and 95 per cent Bayesian credible regions, respectively. In this case these serve as upper limits, as any combination of sufficiently small η and steep κ is consistent with zero HVSs in EDR3. At our fiducial IMF slope, ejection rates in excess of $2 \times 10^{-4} \text{ yr}^{-1}$ can be excluded at $>2\sigma$. Models with an extremely top-heavy IMF such as that suggested by B10 can be discarded unless the HVS ejection rate is lower than $3 \times 10^{-5} \text{ yr}^{-1}$. If the GC IMF is canonical ($\kappa = -2.35$; S55), ejection rates up to 10^{-3} yr^{-1} are still allowed.

In the top right-hand panel of Fig. 5 we show posteriors if only the existence of S5-HVS1 is considered and priors on κ and η are assumed uniform. This observation excludes regions of low η / steep κ , as an S5-HVS1-like object is too rare an outcome from these models. Conversely, if the ejection rate is too large and the IMF too top-heavy, far more than one S5-HVS1 analogue is expected. The strip of models consistent with a single S5-HVS1-like object is degenerate in this space and includes our fiducial model within the 1σ contour.

The bottom left-hand panel of Fig. 5 shows the joint posterior probabilities with uniform priors when both the lack of HVSs in *Gaia* EDR3 and the existence of S5-HVS1 are considered. While no

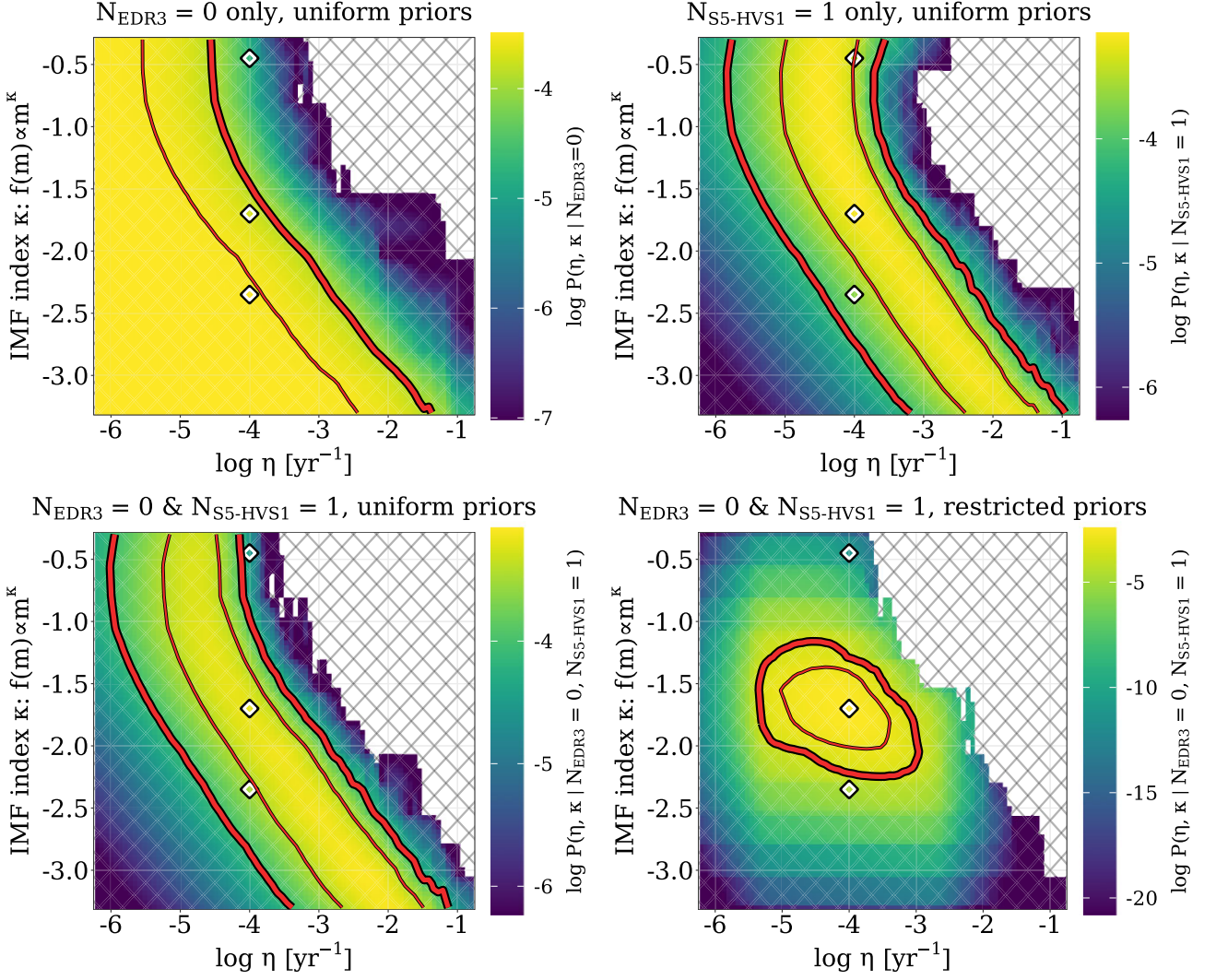


Figure 5. Colourscale shows (log) posterior probabilities for $\kappa - \eta$ model combinations when various data and priors are considered (see Section 3.2 and panel titles). The thin and thick red contours show the 68 per cent and 95 per cent Bayesian credible regions, respectively. The black-and-white diamonds show our fiducial model ($\kappa = -1.7$, $\eta = 10^{-4} \text{ yr}^{-1}$) as well as a model in which $\kappa = -2.3$ (S55), and $\kappa = -0.45$ (B10). The hashed region shows models for which the posterior probability is zero.

IMF slope can be excluded outright due to the degeneracy in this space, an HVS ejection rate above $2 \times 10^{-3} \text{ yr}^{-1}$ can be excluded unless the GC IMF is more top-light than a canonical S55 IMF. A model in which the HVS ejection rate is $\eta = 10^{-4} \text{ yr}^{-1}$ and the IMF is canonical can be excluded at $>1\sigma$ confidence, and a model in which $\eta = 10^{-4} \text{ yr}^{-1}$ and $\kappa = -0.45$ (B10) can be excluded at $>2\sigma$. Our fiducial $\kappa = -1.7$ is consistent with these observations for $\eta = 0.7^{+1.5}_{-0.5} \times 10^{-4} \text{ yr}^{-1}$.

Finally, in the bottom right-hand panel of Fig. 5 we compute posterior distributions with when assuming our set of more restrictive priors. Together, the available HVS observational data and priors motivate a scenario in which $\kappa = -1.8^{+0.4}_{-0.3}$ and $\log[\eta/\text{yr}^{-1}] = -4.1^{+0.6}_{-0.8}$. We point out that with these restrictive priors considered, our fiducial model ($\kappa = -1.7$, $\eta = 10^{-4} \text{ yr}^{-1}$) sits comfortably within the 1σ contour and quite close to the maximum a posteriori model, though this is not surprising given the fact that our fiducial model was chosen in the first place based upon these priors.

In summary, the constraints offered by EDR3 alone upon κ and η improve significantly upon those offered by E22, where only models

in which $\eta \gtrsim 3 \times 10^{-2} \text{ yr}^{-1}$ could be excluded. By considering the existence of S5-HVS1 these constraints tighten further, particularly at low ejection rates and steep IMF slopes. There is no tension between these constraints and existing estimates of κ and η individually.

3.3 Prospects for the future

With the constraints outlined above, we are well-positioned to make specific predictions about the HVS population yet to be uncovered in Gaia DR3 and DR4 and how these unearthed populations may improve constraints even further.

Each coloured band in Fig. 6 shows the region of $\kappa - \eta$ space consistent with a specific number of HVs appearing in Gaia DR3 (left-hand panel) and DR4 (right-hand panel) at the 1σ level. For instance, if 100 high-confidence HVS are discovered in Gaia DR3, the most-pale band shows the $\kappa - \eta$ models for which the $\pm 1\sigma$ range of the predicted HVS population size includes 100. The red lines show the 68 per cent and 95 per cent credible intervals from our modelling constraints when uniform priors are considered on κ

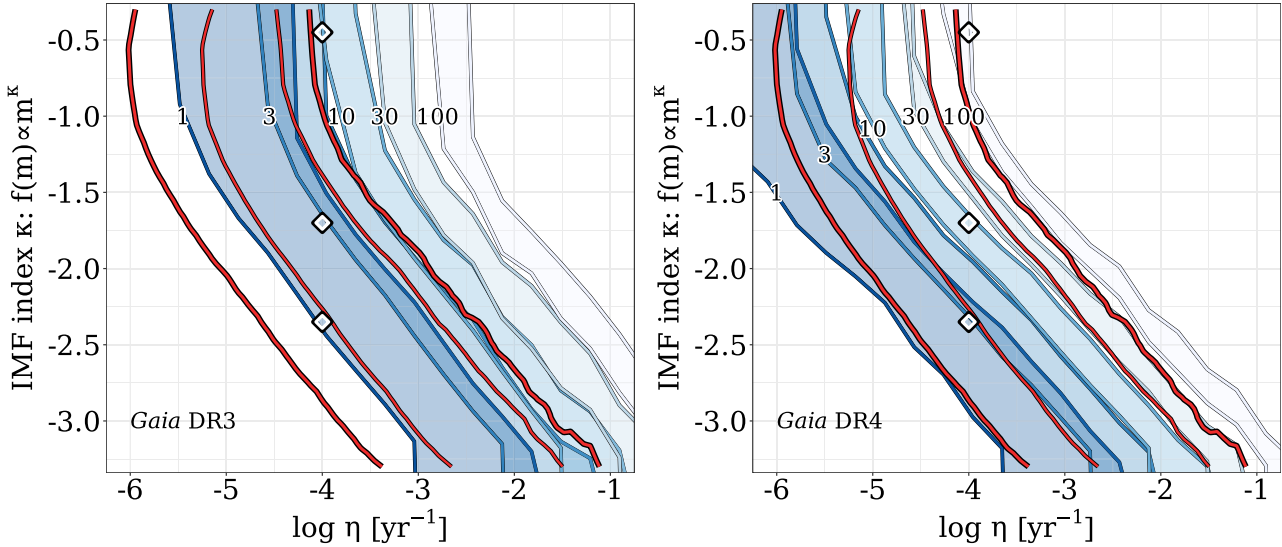


Figure 6. If 1/3/10/30/100 HVSs are discovered in *Gaia* DR3 (left-hand panel) and DR4 (right-hand panel), the shaded coloured regions show the regions of the $\kappa - \eta$ parameter space consistent within 2σ with these findings. The black-and-white diamonds indicate our fiducial ejection rate of $\eta = 10^{-4} \text{ yr}^{-1}$ and fiducial $\kappa = -1.7$ (L13), as well as $\kappa = -2.35$ (S55) and $\kappa = -0.45$ (B10). The red lines indicate the 68 per cent and 95 per cent credible regions for $\kappa - \eta$ as outlined in Section 3.2 when uniform priors are considered.

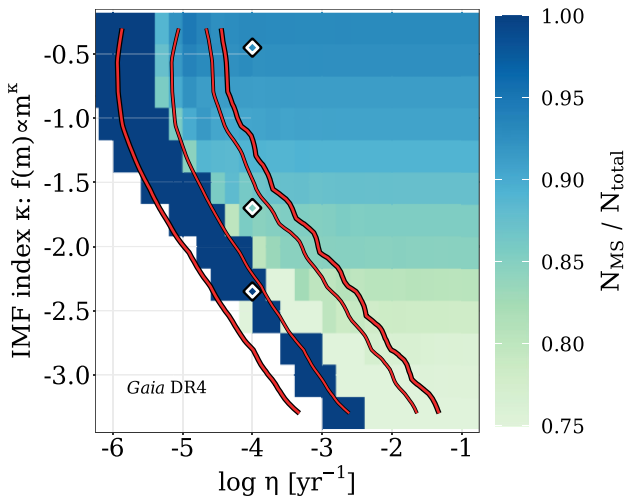


Figure 7. The modal (most frequent) value for the proportion of main sequence HVSs in *Gaia* DR4. The red lines indicate the 68 per cent and 95 per cent credible regions in this parameter space (Fig. 5, lower left-hand panel). The white region shows models for which <1 total HVSs are expected.

and η (Fig. 5, lower left-hand panel). Sampling from this posterior, we predict 0.8 ± 0.7 HVSs will be uncovered in DR3 and $4.9^{+11.2}_{-3.7}$ in DR4. Detecting HVS populations near these expectations will validate our methodology but may only offer modest improvements on model constraints. However, if zero or $\gtrsim 3$ HVSs are detected in DR3 and/or ≤ 3 or $\gtrsim 20$ HVSs are uncovered in DR4, updating posteriors with this new data will significantly change the maximum a posteriori model and tighten constraints considerably.

Our constraints are degenerate in $\kappa - \eta$ space: a larger ejection rate and steep IMF can predict the same number of HVSs as a lower ejection rate and shallower IMF. With *Gaia* DR4 we can begin to break this degeneracy by examining the HVS population in greater detail. While HVSs ejected from the GC will on average be more

massive if the IMF is top-heavy, the spread of HVS stellar masses is large and the detected DR4 HVS population is not likely to be numerous enough to provide insight into the IMF slope using the HVS mass distribution alone. More discriminating are the relative numbers of main sequence and evolved HVSs. We demonstrate this in Fig. 7. Here we show how the modal (most frequently occurring) proportion of main sequence stars among all DR4-detectable HVSs changes in $\kappa - \eta$ space, if ≥ 1 HVSs are expected at all. For the dark blue stripe of models towards lower ejection rates and steep IMFs, we predict only one or two HVSs in DR4 and they are most likely to be on the main sequence. For models in which more HVSs are predicted, the main sequence fraction of HVSs rises more or less monotonically with increasing κ . If, for example, 12 HVSs in total are found in DR4 and 9 are on the main sequence, this would require an IMF no more top-heavy than $\kappa = -1.4$.

4 DISCUSSION

4.1 Concerns, caveats, and alternative assumptions

The modelling and analysis presented here depends on a number of assumptions concerning the properties of stellar binaries in the GC, the mechanism of HVS ejection, and the observational capabilities of *Gaia*. In this subsection we comment on several of these assumptions and their impact on our results.

One assumption we have made here is that the Hills mechanism is solely responsible for HVS ejections from the GC – the constraints on the GC stellar environment we present here apply exclusively to a Hills ejection scenario. While this is the most popular HVS ejection mechanism from the GC, alternative scenarios exist involving e.g. an as-of-yet undetected supermassive or intermediate-mass black hole companion to Sgr A* (e.g. Yu & Tremaine 2003; Gualandris, Portegies Zwart & Sipior 2005; Sesana, Haardt & Madau 2006, 2007; Darbha et al. 2019; Rasskazov et al. 2019; Zheng, Lin & Mao 2021), a population of stellar mass black holes in the GC (O’Leary & Loeb 2007), the disruption of infalling globular clusters (Capuzzo-

Dolcetta & Fragione 2015; Fragione & Capuzzo-Dolcetta 2016), or supernovae within GC binaries (Zubovas, Wynn & Gualandris 2013; Bortolas, Mapelli & Spera 2017; Hoang, Naoz & Stoneker 2022). Each of these mechanisms, if exclusively or partially responsible for HVSs, would warrant a different approach to the ejection model.

In predicting the future *Gaia* HVS population, we have assumed that astrometric and spectroscopic solutions will have zero systematic error (see discussion in E22) and that the detected HVS population will not be contaminated by fast stars ejected from outside the GC. In E22 Appendix B we show that the latter is not a pressing concern – 90 to 95 per cent of HVSs detectable by *Gaia* will have trajectories which unambiguously suggest an origin in the GC.

In this work, we have assumed that the mass ratios (q) among GC binaries follow a power-law distribution, i.e. $f(q) \propto q^\gamma$, where in each iteration γ is drawn at random in the interval $[-2, +2]$. A feature we have not allowed in this distribution is the so-called ‘twin’ phenomenon – the observed statistical excess of equal or nearly equal-mass binary systems across a range of total mass and orbital separation ($q \gtrsim 0.95$) (Lucy & Ricco 1979; Tokovinin 2000; Moe & Di Stefano 2017; El-Badry et al. 2019). We test the impact of this feature by running another suite of simulations in the extreme case in which *all* binaries in the GC are equal-mass. While our predictions for *Gaia* DR4 change slightly ($18.5^{+4.6}_{-4.4}$ total HVSs in our fiducial model compared to $10.9^{+4.8}_{-4.2}$ in our original prescription), the constraints on the GC IMF and HVS ejection rate from *Gaia* EDR3 and S5-HVS1 remain largely unchanged.

We assess the impact of the IMF functional form with a similar test. We have assumed a single power-law in this work ($f(m) \propto m^\kappa$), while other canonical IMFs have broken power law (Kroupa 2001) or lognormal (Chabrier 2003) forms. Modern infrared observations of the GC (B10, L13) are not sensitive to low-mass stars, so they cannot constrain a change in the IMF slope in the subsolar regime. We run yet another suite of simulations where we vary the IMF slope only in the $m \geq 0.5 M_\odot$ regime and the IMF log-slope remains fixed at -1.3 in the range $0.08 M_\odot \leq m < 0.5 M_\odot$ (Kroupa 2001). Constraints from *Gaia* EDR3 and S5-HVS1 become slightly more vertical in $\kappa - \eta$ space as we now expect more (fewer) HVSs for $\kappa < -1.3$ ($\kappa > -1.3$) when compared to a single power law, but otherwise remain unchanged. For our fiducial model, this prescription would predict $14.2^{+5.8}_{-5.0}$ total HVSs in *Gaia* DR4.

Throughout this work we have assumed a constant HVS ejection rate and, implicitly, a constant star formation rate in the GC. In our fiducial model ($\kappa = -1.7$, $\eta = 10^{-4} \text{ yr}^{-1}$), only stars with $t_{\text{flight}} \lesssim 20 \text{ Myr}$ would be bright enough to appear in any *Gaia* data release with precise astrometry and a measured radial velocity, and only HVSs with $t_{\text{flight}} \lesssim 65 \text{ Myr}$ would be bright enough to appear in S⁵ as an S5-HVS1 analogue. Our constraints on η in this work can be therefore thought of as applying only to the typical ejection rate over the last few tens of Myr, since we base these constraints only on (un-)observed HVSs ejected in the relatively recent past. By a similar token, only the GC star formation history within the last $\sim 0.5 \text{ Gyr}$ is relevant for this work – HVSs older than this would not be detectable in both *Gaia* EDR3 and S⁵. While there is evidence suggesting that the star formation rate in the GC has been non-continuous throughout the history of the Galaxy and has in fact increased slightly within the last $\sim 100 \text{ Myr}$ (Pfuhl et al. 2011; Nogueras-Lara et al. 2020), a constant star formation rate within the last 0.5 Gyr is a reasonable assumption (see also Figer et al. 2004).

Stars age in our model according to standard single stellar evolution prescriptions. While binary interactions can be ignored since we have required that HVS progenitor binaries remain sufficiently well-

separated, the extremity of the GC environment may still influence stellar evolution. Of particular interest is nuclear activity from Sgr A*. ~ 40 per cent of *Gaia* EDR3-detectable HVSs in our fiducial model were ejected within the last 8 Myr, and evidence for a Seyfert-level flare from the GC $\sim 2\text{--}8 \text{ Myr}$ ago has been mounting in recent years (see Bland-Hawthorn et al. 2019; Cecil et al. 2021, and references therein). Active galactic nuclei (AGNs) are known to impact the evolution of stars within them – accretion from the AGN gas disc can extend the hydrogen-burning lifetime of low-mass stars and increase their total mass (Cantiello, Jermyn & Lin 2021; Dittmann, Cantiello & Jermyn 2021; Jermyn et al. 2022). If prior episodes of nuclear activity in the GC have impacted a non-negligible fraction of HVS progenitor binaries, then their evolutionary states and apparent magnitudes may be inaccurately estimated.

One assumption in our model is that HVSs are equally likely to be ejected at any point during their lifetime. This is motivated by the fact that existing HVS candidates do not appear to be biased towards particular ages. We also assume that the IMF among the primaries of HVS progenitor binaries matches the IMF of stars in the GC region as a whole, and that this IMF remains constant in time. These assumptions mean that some massive *Gaia*-detectable mock HVSs in our simulations must be ejected quite shortly after formation. Among (E)DR3-visible HVSs, the typical age of an HVS at the moment of ejection is 100 Myr. Among DR4-visible HVSs, however, these median age at ejection drops to only $\sim 10 \text{ Myr}$. Theoretical works indicate that diffusing a binary into the Sgr A* loss cone to soon after formation may be problematic (Yu & Tremaine 2003; Merritt & Poon 2004; Wang & Merritt 2004; Perets et al. 2007). If an unrealistic number of young HVSs are being ejected in our model, predictions for the *Gaia* DR4 HVS population may be overestimated.

4.2 Previous work and other HVS (non-)detections

Prior works have used HVS non-detections to constrain the GC ejection rate. Kollmeier et al. (2009) infer an ejection rate for HVSs of spectral type F and G of $\eta_F < 6 \times 10^{-5} \text{ yr}^{-1}$ and $\eta_G < 3 \times 10^{-4} \text{ yr}^{-1}$, respectively, upon finding zero old, unbound HVS candidates among stars with measured radial velocities in the Sloan Digital Sky Survey (SDSS; York et al. 2000). Our results are consistent with these constraints – at our fiducial κ , our constraints in the lower left-hand panel of Fig. 5 indicate $\eta_F \lesssim 8 \times 10^{-5} \text{ yr}^{-1}$ at 2σ confidence and $\eta_G \lesssim 6 \times 10^{-5} \text{ yr}^{-1}$. Kollmeier et al. (2010) similarly find zero metal-rich old HVSs in SEGUE-2 (Yanny et al. 2009). They deduce that the ejection rate of 5 Gyr-old, solar-metallicity HVSs which reach a Galactocentric velocity of 500 km s^{-1} at the Solar circle is $< 4.1 \times 10^{-4} \text{ yr}^{-1}$ per logarithmic unit of stellar mass, again consistent with this work. Notably, Kollmeier et al. (2010) also conclude that the GC ejects ~ 5.5 times as many F/G stars as B stars, corresponding to a quite top-heavy GC IMF ($\kappa \approx -0.6$).

In principle, HVS null detections (to date) in other ground-based surveys such as RAVE (Steinmetz et al. 2006), LAMOST (Zhao et al. 2012), GALAH (De Silva et al. 2015), APOGEE (Majewski et al. 2017), and H3 (Conroy et al. 2019) could also be used to place constraints on the GC stellar environment. Properly considering HVS non-detections in all these surveys combined would require careful modelling of each individual survey’s selection function and observational systematics, with no guarantee that constraints would improve relative to those provided by *Gaia* alone. The advantage of *Gaia* is its coverage, its catalogue size, its (relatively) well-modelled

spectroscopic selection function and its ability to measure 3D velocities without complementary observations from other surveys – we focus on it here and defer a holistic treatment of all available Galactic surveys to future work.

Another option is to consider the HVS candidates in the MMT HVS Survey (Brown, Geller & Kenyon 2009; Brown et al. 2014), which uncovered tens of HVS candidates by targeting $[2.5, 4] M_{\odot}$ stars in SDSS for follow-up spectroscopic observation. While it is relatively straightforward to select analogues for these candidates from among our mock HVS samples using the SDSS footprint and mock SDSS photometry, it is unclear how many and which MMT HVS candidates are genuine GC-ejected HVSs. A GC origin remains plausible for a \sim dozen candidates in the MMT HVS Survey (see Brown et al. 2018; Irrgang et al. 2018; Kreuzer et al. 2020), however, the distribution of possible ejection locations for many candidates is many times larger than the entire Galactic disc. While valuable analyses can be done assuming all of these candidates are genuine HVSs (e.g. Kollmeier et al. 2009, 2010; Rossi et al. 2017), due to this ambiguity we opt not to consider the MMT HVS Survey when testing our model predictions.

4.3 Hypervelocity curios

4.3.1 Hypervelocity standard candles

A keen-eyed reader may notice that a minority population of HVS candidates in *Gaia* DR3 and DR4 are core helium-burning stars currently on a blue loop phase of evolution (see Fig. 4). Many such stars will cross the so-called instability strip; stars in this region of the Hertzsprung–Russell diagram are unstable to radial oscillations and may stand out as classical Cepheid variable stars.

Due to the correlation between their pulsational periods and intrinsic luminosities (Leavitt & Pickering 1912), heliocentric distances to *Gaia* Cepheids can currently be determined to a precision of a few per cent (see Owens et al. 2022). With such precise distance estimations, the birthplaces, and Galactocentric velocities of hypervelocity Cepheid (HVC) candidates can be tightly constrained. HVCs appearing in the *Gaia* radial velocity catalogues would therefore not need to satisfy our strict 20 per cent relative parallax error cut to be identified as a high-quality HVS candidate. Furthermore, a radial velocity measurement may not even be necessary for HVCs with large tangential velocities: with a precise distance estimate, uncertainties on tangential velocities will be small and the HVS candidate’s origin can be well-constrained even in the absence of full 3D velocity information. In our fiducial model we predict $1.9^{+1.2}_{-1.0}$ HVCs to appear in the DR4 source catalogue ($G < 20.7$). Of these, however, only $1.1^{+1.2}_{-0.9}$ will be bright enough to appear in the radial velocity catalogue. Therefore, while prospects are not particularly promising, with some luck DR4 may supply the first known GC-ejected hypervelocity standard candle.

We note as well that a significant fraction of HVSs detectable in *Gaia* DR3 and DR4 reside in the so-called ‘red clump’ at $T_{\text{eff}} \sim 5000$ K and $L \sim 100 L_{\odot}$ (Fig. 4), corresponding to low-mass core helium-burning stars (see Girardi 2016, for a review). With its roughly fixed absolute magnitude, the red clump can be used as a standard candle to measure distances (Cannon 1970). Since *Gaia* HVSs will be located all across the sky in regions of differing extinction, calibrating a clean red clump HVS sample using *Gaia* optical photometry alone is unfeasible. This does, however, support the attractive possibility of searching for red clump HVSs in cross-matched combinations of *Gaia* with infrared Galactic surveys (see Luna et al. 2019).

4.3.2 Hypervelocity supernovae

Within this work we have shown that there exists a population of HVSs in the Galaxy which are at late stages of stellar evolution. It is natural, then, to wonder about the deaths of these HVSs. Massive ($m \gtrsim 8 M_{\odot}$) HVSs may undergo core-collapse supernovae (CCSNe) whose explosion or remnant could be detected. It is important to note, however, that not all core-collapse events can be associated with a supernova explosion. A significant fraction may collapse directly to a black hole without a luminous electromagnetic signature (Kochanek et al. 2008). The precise outcome for a $m_{\text{ZAMS}} \gtrsim 14 M_{\odot}$ core-collapse event depends intimately on subtle aspects of its progenitor star’s structure in its final moments – a simple mapping between progenitor and outcome does not exist (O’Connor & Ott 2011; Pejcha & Thompson 2015; Ertl et al. 2016; Sukhbold et al. 2016) and robustly modelling this is beyond the scope of this work. Regardless, with some simple assumptions we can use our simulation framework to explore the occurrence of hypervelocity supernovae (HVSNe) in the Galaxy.

Since stars which do not survive until the present day are removed in our methodology as described in Section 2, we perform another suite of simulations. Using the same $\kappa - \eta$ model grid, we eject and propagate only $m > 8 M_{\odot}$ stars which were main sequence or evolved stars at time of ejection, but are compact remnants today according to our stellar evolution prescription. We make the simple assumption that $m_{\text{ZAMS}} \geq 20 M_{\odot}$ stars tend to implode rather than go supernova (see Ertl et al. 2016; Sukhbold, Woosley & Heger 2018; Sukhbold & Adams 2020), and we remove them for the sample. A star evolves as it is propagated through the Galactic potential, and we end the orbital integration at the first timestep in which the star is a compact remnant. The star is assumed to undergo a CCSNe at this time and we record the location in the Galaxy and the lookback time t_{lb} ago at which this happened.

We show the results of this investigation in Fig. 8. The top panel shows the cumulative distribution of t_{lb} over the last 100 Myr. Our fiducial model predicts that 75^{+31}_{-23} core-collapse HVSNe have occurred during this time period, with only $1.0^{+1.1}_{-0.8}$ occurring within the last Myr. Assuming the rate of CCSNe in the Milky Way is $\sim [1 - 2] \times 10^{-2} \text{ yr}^{-1}$ (see Rozwadowska, Vissani & Cappellaro 2021, and references therein), HVSNe then represent $\sim 0.005 - 0.01$ per cent of Galactic CCSNe. In the bottom panels of Fig. 8 we show the locations of $t_{\text{lb}} < 1$ Myr in the Galaxy in Galactocentric Cartesian x – z plane (left-hand panel) and x – y plane (right-hand panel), stacked over 100 iterations. The blue arrows indicate the Galactocentric velocity of the HVSNe progenitor star at the moment of core collapse. While most HVSNe occur in the inner few kpc of the Galaxy arising from short-lived massive stars, nearly half will be offset from the Galactic disc by 10 kpc or more. These events would be characterized by their exceptional line of sight: 7 in 10 HVSNe would satisfy $|v_{\text{rad}}| \geq 800 \text{ km s}^{-1}$.

While Galactic HVSNe are quite rare, they invite the prospect of observing HVSNe in other galaxies. New and ongoing transient surveys such as the Zwicky Transient Facility Bright Transient Survey (Fremling et al. 2020; Perley et al. 2020), the All Sky Automated Survey for Supernovae (Shappee et al. 2014), and the Asteroid Terrestrial-impact Last Alert System (Tonry et al. 2018) scan the optical sky nearly nightly and to date have observed \sim hundreds of extragalactic CCSNe in the local ($z \lesssim 0.1$) Universe. With the Rubin Observatory’s upcoming Legacy Survey of Space and Time (Ivezic et al. 2019), this rate of CCSNe detections is expected to increase tenfold. Extragalactic HVSNe might be uncovered in such surveys by searching for events significantly offset from the disc

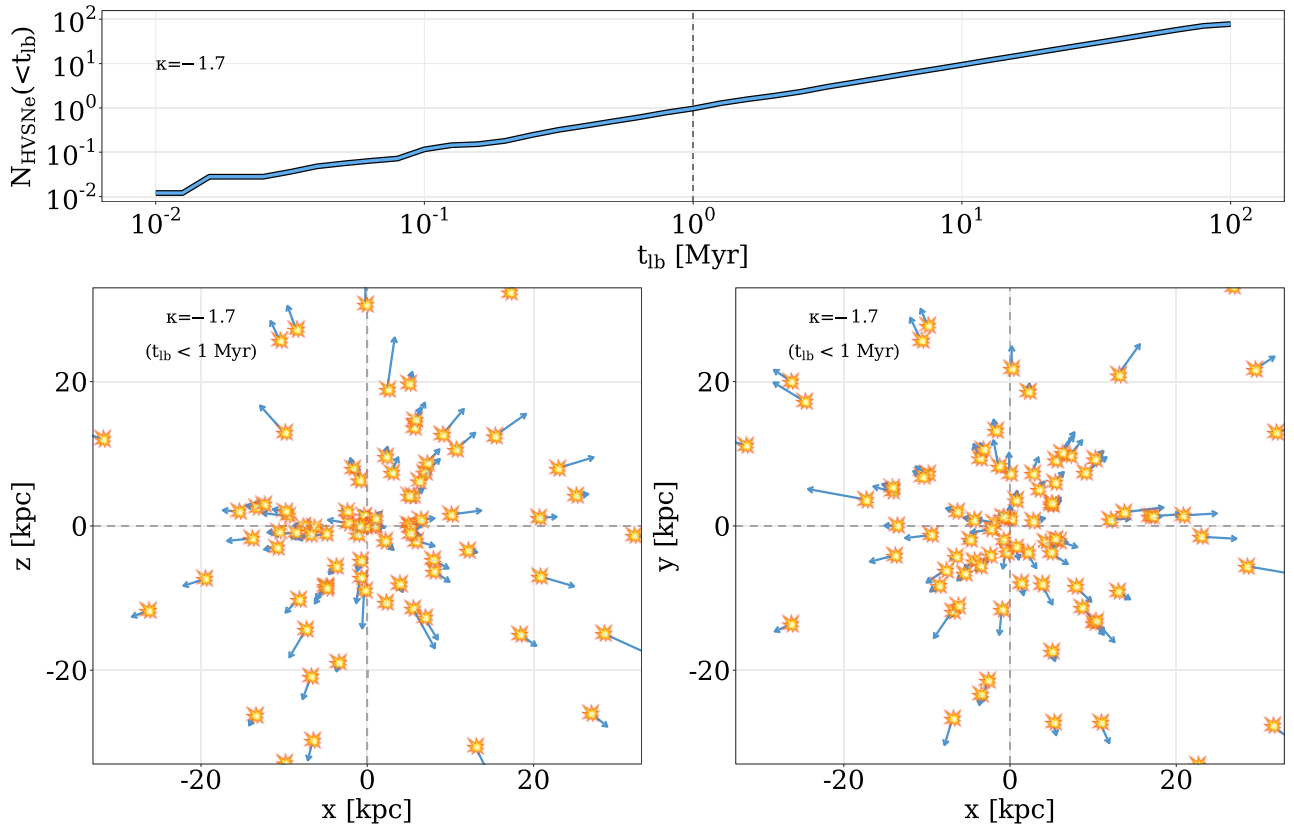


Figure 8. Top: Cumulative distribution of hypervelocity supernovae (HVSNe) lookback times t_{lb} in our fiducial model. The dashed vertical line indicates $t_{\text{lb}} = 1$ Myr ago. Bottom: The locations of HVSNe occurring within the last Myr in the Galactocentric Cartesian x - z (left-hand panel) and x - y (right-hand panel) planes, stacked over 50 runs. The blue vectors indicate the velocity of the progenitor HVS at the moment of core collapse.

of their host and/or with significant peculiar velocities with respect to their host. The initial mass functions and HVS ejection rates within the nuclei of external galaxies will depend on their accretion history, star formation history, and history of nuclear activity. Such HVSNe observations would be the first observational evidence of hypervelocity ejections outside the Local Group and would join tidal disruption event rate observations (see Bortolas 2022) as a valuable tool for directly investigating the nuclei of galaxies in the local Universe.

5 CONCLUSIONS

In this work, we simulate the ejection of hypervelocity stars (HVSs) from the Galactic Centre (GC) via the tidal breakup of stellar binaries following dynamical encounters with Sgr A*. We expand upon the previous work of Evans et al. (2022) by investigating evolved HVSs as well as main sequence ones, as these evolved HVSs would more easily appear in current data releases from the European Space Agency’s *Gaia* mission. By considering that lack of known HVSs in *Gaia* EDR3 with precise astrometry and radial velocities as well as the existence of the HVS candidate S5-HVS1 (Koposov et al. 2020), we place robust and competitive constraints on the stellar IMF among the primaries of HVS progenitor binaries and the ejection rate of HVSs from the GC. Using these constraints, we make predictions about the evolved and main sequence HVS populations to appear in upcoming *Gaia* data releases.

Our findings can be summarized as follows:

(i) For a fiducial model in which the IMF is a single power law ($f(m) \propto m^\kappa$) with $\kappa = -1.7$ (Lu et al. 2013) and the HVS ejection rate η is 10^{-4} yr^{-1} (see Brown 2015), <1 high-confidence HVSs in total are expected in the radial velocity catalogues of *Gaia* DR2 and EDR3. This is consistent with observations (e.g. Hattori et al. 2018; Marchetti et al. 2018; Marchetti 2021) (Fig. 2).

(ii) Predicted numbers of observed HVSs in all *Gaia* data releases are degenerate in the IMF index-ejection rate parameter space (Fig. 3 and following figures).

(iii) For $\kappa = -1.7$, the lack of GC-ejected HVS candidates in *Gaia* EDR3 disfavors ejection rates above $2 \times 10^{-4} \text{ yr}^{-1}$. Larger ejection rates are only allowed if the IMF is top-light (upper left-hand panel of Fig. 5).

(iv) Accounting as well for the existence of the S5-HVS1, we obtain tighter constraints that additionally exclude the low ejection rate–bottom-light IMF region of the parameter space (lower left-hand panel of Fig. 5). At $\kappa = -1.7$ the evidence favours an HVS ejection rate of $\eta = 0.7_{-0.5}^{+1.5} \times 10^{-4} \text{ yr}^{-1}$. This favoured ejection rate grows (shrinks) as the IMF becomes more bottom-heavy (top-heavy).

(v) Our derived constraints predict 0.8 ± 0.7 HVSs to be present in the *Gaia* DR3 radial velocity catalogue with precise astrometry, and $4.9_{-3.7}^{+11.2}$ in *Gaia* DR4. The majority of DR3 HVSs will be core helium-burning, while main sequence HVSs will dominate in DR4 (Figs 2 and 6).

With this work and with E22, we have shown that where HVSs are not is equally as interesting as where they are. We have demonstrated in this work that evolved HVSs in the context of *Gaia* are a powerful

tool for constraining the GC environment. This work shows that competitive constraints on the stellar initial mass function and HVS ejection rate in the GC can be gleaned from a small number of HVS (non-)detections. With future *Gaia* data releases and with complementary upcoming Galactic spectroscopic surveys such as WEAVE (Dalton et al. 2012) and 4MOST (de Jong et al. 2019), HVS observations will gain even more prominence as an avenue for studying the supermassive black hole at the centre of our Galaxy and its interactions with its environment.

ACKNOWLEDGEMENTS

The authors thank the anonymous referee for their valuable feedback. They also wish to Anthony Brown and Rainier Schödel for helpful comments and Sergey Koposov, Warren Brown, Sill Verberne, and Alonso Luna for enlightening conversations. FAE acknowledges funding support from the Natural Sciences and Engineering Research Council of Canada (NSERC) Postgraduate Scholarship. TM acknowledges an ESO fellowship. EMR acknowledges that this project has received funding from the European Research Council (ERC) under the European Union's Horizon 2020 research and innovation programme (Grant agreement No. 101002511 - VEGA P).

DATA AVAILABILITY

The simulation outputs underpinning this work can be shared upon reasonable request to the corresponding author. These simulations were produced using the SPEEDYSTAR package, publicly available at <https://github.com/fraserevans/speedystar>.

REFERENCES

- Abbott T. M. C. et al., 2018, *ApJS*, 239, 18
 Asplund M., Grevesse N., Sauval A. J., Scott P., 2009, *ARA&A*, 47, 481
 Bailer-Jones C. A. L., 2015, *PASP*, 127, 994
 Barnard E. E., 1916, *AJ*, 29, 181
 Bartko H. et al., 2010, *ApJ*, 708, 834 (B10)
 Bessell M. S., 1990, *PASP*, 102, 1181
 Blaauw A., 1961, *Bull. Astron. Inst. Netherlands*, 15, 265
 Bland-Hawthorn J. et al., 2019, *ApJ*, 886, 45
 Boersma J., 1961, *Bull. Astron. Inst. Netherlands*, 15, 291
 Bortolas E., 2022, *MNRAS*, 511, 2885
 Bortolas E., Mapelli M., Spera M., 2017, *MNRAS*, 469, 1510
 Boubert D., Everall A., 2020, *MNRAS*, 497, 4246
 Boubert D., Guillochon J., Hawkins K., Ginsburg I., Evans N. W., Strader J., 2018, *MNRAS*, 479, 2789
 Boubert D. et al., 2019, *MNRAS*, 486, 2618
 Boubert D., Everall A., Holl B., 2020, *MNRAS*, 497, 1826
 Bovy J., 2015, *ApJS*, 216, 29
 Bovy J., Rix H.-W., Green G. M., Schlafly E. F., Finkbeiner D. P., 2016, *ApJ*, 818, 130
 Bromley B. C., Kenyon S. J., Geller M. J., Barcikowski E., Brown W. R., Kurtz M. J., 2006, *ApJ*, 653, 1194
 Bromley B. C., Kenyon S. J., Geller M. J., Brown W. R., 2012, *ApJ*, 749, L42
 Bromley B. C., Kenyon S. J., Brown W. R., Geller M. J., 2018, *ApJ*, 868, 25
 Brown W. R., 2015, *ARA&A*, 53, 15
 Brown A. G. A., 2019, in *The Gaia Universe*. p. 18
 Brown W. R., Geller M. J., Kenyon S. J., Kurtz M. J., 2005, *ApJ*, 622, L33
 Brown W. R., Geller M. J., Kenyon S. J., Kurtz M. J., 2006, *ApJ*, 640, L35
 Brown W. R., Geller M. J., Kenyon S. J., Kurtz M. J., Bromley B. C., 2007, *ApJ*, 660, 311
 Brown W. R., Geller M. J., Kenyon S. J., 2009, *ApJ*, 690, 1639
 Brown W. R., Geller M. J., Kenyon S. J., 2012, *ApJ*, 751, 55
 Brown W. R., Geller M. J., Kenyon S. J., 2014, *ApJ*, 787, 89
 Brown W. R., Anderson J., Gnedin O. Y., Bond H. E., Geller M. J., Kenyon S. J., 2015, *ApJ*, 804, 49
 Brown W. R., Lattanzi M. G., Kenyon S. J., Geller M. J., 2018, *ApJ*, 866, 39
 Cannon R. D., 1970, *MNRAS*, 150, 111
 Cantiello M., Jermyn A. S., Lin D. N. C., 2021, *ApJ*, 910, 94
 Capuzzo-Dolcetta R., Fragione G., 2015, *MNRAS*, 454, 2677
 Cardelli J. A., Clayton G. C., Mathis J. S., 1989, *ApJ*, 345, 245
 Cecil G., Wagner A. Y., Bland-Hawthorn J., Bicknell G. V., Mukherjee D., 2021, *ApJ*, 922, 254
 Chabrier G., 2003, *PASP*, 115, 763
 Choi J., Dotter A., Conroy C., Cantiello M., Paxton B., Johnson B. D., 2016, *ApJ*, 823, 102
 Conroy C. et al., 2019, *ApJ*, 883, 107
 Contigiani O., Rossi E. M., Marchetti T., 2019, *MNRAS*, 487, 4025
 Cropper M. et al., 2018, *A&A*, 616, A5
 Dalton G. et al., 2012, in McLean I. S., Ramsay S. K., Takami H., eds, *Proc. SPIE Conf. Ser. Vol. 8446, Ground-based and Airborne Instrumentation for Astronomy IV*. SPIE, Bellingham, p. 84460P
 Darbha S., Coughlin E. R., Kasen D., Quataert E., 2019, *MNRAS*, 482, 2132
 de Jong R. S. et al., 2019, *The Messenger*, 175, 3
 De Silva G. M. et al., 2015, *MNRAS*, 449, 2604
 Deason A. J., Fattahi A., Belokurov V., Evans N. W., Grand R. J. J., Marinacci F., Pakmor R., 2019, *MNRAS*, 485, 3514
 Dittmann A. J., Cantiello M., Jermyn A. S., 2021, *ApJ*, 916, 48
 Do T., Lu J. R., Ghez A. M., Morris M. R., Yelda S., Martinez G. D., Wright S. A., Matthews K., 2013, *ApJ*, 764, 154
 Do T., Kerzendorf W., Winsor N., Støstad M., Morris M. R., Lu J. R., Ghez A. M., 2015, *ApJ*, 809, 143
 Dormand J., Prince P., 1980, *J. Comput. Appl. Math.*, 6, 19
 Dotter A., 2016, *ApJS*, 222, 8
 Du C., Li H., Yan Y., Newberg H. J., Shi J., Ma J., Chen Y., Wu Z., 2019, *ApJS*, 244, 4
 Dunstall P. R. et al., 2015, *A&A*, 580, A93
 Edelmann H., Napiwotzki R., Heber U., Christlieb N., Reimers D., 2005, *ApJ*, 634, L181
 Eggleton P. P., 1983, *ApJ*, 268, 368
 Eisenhauer F. et al., 2005, *ApJ*, 628, 246
 El-Badry K., Rix H.-W., Tian H., Duchêne G., Moe M., 2019, *MNRAS*, 489, 5822
 Eldridge J. J., Langer N., Tout C. A., 2011, *MNRAS*, 414, 3501
 Erkal D., Boubert D., Gualandris A., Evans N. W., Antonini F., 2019, *MNRAS*, 483, 2007
 Ertl T., Janka H. T., Woosley S. E., Sukhbold T., Ugliano M., 2016, *ApJ*, 818, 124
 Evans F. A., Renzo M., Rossi E. M., 2020, *MNRAS*, 497, 5344
 Evans F. A., Marchetti T., Rossi E. M., Baggen J. F. W., Bloot S., 2021, *MNRAS*, 507, 4997
 Evans F. A., Marchetti T., Rossi E. M., 2022, *MNRAS*, 512, 2350 (E22)
 Everall A., Boubert D., 2022, *MNRAS*, 509, 6205
 Everall A., Boubert D., Koposov S. E., Smith L., Holl B., 2021, *MNRAS*, 502, 1908
 Feldmeier-Krause A., Kerzendorf W., Neumayer N., Schödel R., Noguera-Lara F., Do T., de Zeeuw P. T., Kuntschner H., 2017, *MNRAS*, 464, 194
 Feldmeier-Krause A. et al., 2020, *MNRAS*, 494, 396
 Figer D. F., Rich R. M., Kim S. S., Morris M., Serabyn E., 2004, *ApJ*, 601, 319
 Fragione G., Capuzzo-Dolcetta R., 2016, *MNRAS*, 458, 2596
 Fremling C. et al., 2020, *ApJ*, 895, 32
 Gaia Collaboration 2016a, *A&A*, 595, A2
 Gaia Collaboration 2016b, *A&A*, 595, A1
 Gaia Collaboration 2018, *A&A*, 616, A1
 Gaia Collaboration 2021a, *A&A*, 649, A1
 Gaia Collaboration 2021b, *A&A*, 649, A1

- Gaia Collaboration 2022, preprint ([arXiv:2208.00211](https://arxiv.org/abs/2208.00211))
- Generozov A., 2021, *MNRAS*, 501, 3088
- Generozov A., Madigan A.-M., 2020, *ApJ*, 896, 137
- Genzel R., Eisenhauer F., Gillessen S., 2010, *Rev. Mod. Phys.*, 82, 3121
- Ghez A. M. et al., 2008, *ApJ*, 689, 1044
- Gillessen S., Eisenhauer F., Trippe S., Alexander T., Genzel R., Martins F., Ott T., 2009, *ApJ*, 692, 1075
- Gillessen S. et al., 2017, *ApJ*, 837, 30
- Girardi L., 2016, *ARA&A*, 54, 95
- Gnedin O. Y., Gould A., Miralda-Escudé J., Zentner A. R., 2005, *ApJ*, 634, 344
- Gould A., Quillen A. C., 2003, *ApJ*, 592, 935
- Gualandris A., Portegies Zwart S., Sipior M. S., 2005, *MNRAS*, 363, 223
- Gvaramadze V. V., Gualandris A., Portegies Zwart S., 2009, *MNRAS*, 396, 570
- Habibi M. et al., 2017, *ApJ*, 847, 120
- Hattori K., Valluri M., Bell E. F., Roederer I. U., 2018, *ApJ*, 866, 121
- Heber U., Edelmann H., Napiwotzki R., Altmann M., Scholz R.-D., 2008, *A&A*, 483, L21
- Hills J. G., 1988, *Nature*, 331, 687
- Hirsch H. A., Heber U., O'Toole S. J., Bresolin F., 2005, *A&A*, 444, L61
- Hoang B.-M., Naoz S., Sloneker M., 2022, *ApJ*, 934, 54
- Hurley J. R., Pols O. R., Tout C. A., 2000, *MNRAS*, 315, 543
- Irrgang A., Przybilla N., Heber U., Nieva M. F., Schuh S., 2010, *ApJ*, 711, 138
- Irrgang A., Kreuzer S., Heber U., 2018, *A&A*, 620, A48
- Irrgang A., Geier S., Heber U., Kupfer T., Fürst F., 2019, *A&A*, 628, L5
- Ivezić, Ž. et al., 2019, *ApJ*, 873, 111
- Jermyn A. S., Dittmann A. J., McKernan B., Ford K. E. S., Cantiello M., 2022, *ApJ*, 929, 133
- Jordi C. et al., 2010, *A&A*, 523, A48
- Katz D. et al., 2019, *A&A*, 622, A205
- Kenyon S. J., Bromley B. C., Geller M. J., Brown W. R., 2008, *ApJ*, 680, 312
- Kenyon S. J., Bromley B. C., Brown W. R., Geller M. J., 2014, *ApJ*, 793, 122
- Kobayashi S., Hainick Y., Sari R., Rossi E. M., 2012, *ApJ*, 748, 105
- Kochanek C. S., Beacom J. F., Kistler M. D., Prieto J. L., Stanek K. Z., Thompson T. A., Yüksel H., 2008, *ApJ*, 684, 1336
- Kollmeier J. A., Gould A., Knapp G., Beers T. C., 2009, *ApJ*, 697, 1543
- Kollmeier J. A. et al., 2010, *ApJ*, 723, 812
- Koposov S. E. et al., 2020, *MNRAS*, 491, 2465
- Koppelman H. H., Helmi A., 2021, *A&A*, 649, A136
- Kreuzer S., Irrgang A., Heber U., 2020, *A&A*, 637, A53
- Kroupa P., 2001, *MNRAS*, 322, 231
- Launhardt R., Zylka R., Mezger P. G., 2002, *A&A*, 384, 112
- Leavitt H. S., Pickering E. C., 1912, *Harv. Coll. Obs. Circ.*, 173, 1
- Leonard P. J. T., 1991, *AJ*, 101, 562
- Leonard P. J. T., Duncan M. J., 1990, *AJ*, 99, 608
- Li T. S. et al., 2019, *MNRAS*, 490, 3508
- Li Y.-B. et al., 2021, *ApJS*, 252, 3
- Lu J. R., Do T., Ghez A. M., Morris M. R., Yelda S., Matthews K., 2013, *ApJ*, 764, 155 (L13)
- Lucy L. B., Ricco E., 1979, *AJ*, 84, 401
- Luna A., Minniti D., Alonso-García J., 2019, *ApJ*, 887, L39
- Madigan A.-M., Levin Y., Hopman C., 2009, *ApJ*, 697, L44
- Madigan A.-M., Pfuhl O., Levin Y., Gillessen S., Genzel R., Perets H. B., 2014, *ApJ*, 784, 23
- Majewski S. R. et al., 2017, *AJ*, 154, 94
- Maness H. et al., 2007, *ApJ*, 669, 1024
- Marchetti T., 2021, *MNRAS*, 503, 1374
- Marchetti T., Contigiani O., Rossi E. M., Albert J. G., Brown A. G. A., Sesana A., 2018, *MNRAS*, 476, 4697
- Marchetti T., Rossi E. M., Brown A. G. A., 2019, *MNRAS*, 490, 157
- Marchetti T., Evans F. A., Rossi E. M., 2022, *MNRAS*, 515, 767
- McMillan P. J., 2017, *MNRAS*, 465, 76
- Merritt D., Poon M. Y., 2004, *ApJ*, 606, 788
- Moe M., Di Stefano R., 2015, *ApJ*, 810, 61
- Moe M., Di Stefano R., 2017, *ApJS*, 230, 15
- Moe M., Stefano R. D., 2013, *ApJ*, 778, 95
- Necib L., Lin T., 2022, *ApJ*, 926, 189
- Neumayer N., Seth A., Böker T., 2020, *A&AR*, 28, 4
- Nogueras-Lara F. et al., 2020, *Nat. Astron.*, 4, 377
- O'Connor E., Ott C. D., 2011, *ApJ*, 730, 70
- O'Leary R. M., Loeb A., 2007, *MNRAS*, 383, 86
- Oh S., Kroupa P., 2016, *A&A*, 590, A107
- Oort J. H., 1926, PhD thesis, Publications of the Kapteyn Astronomical Laboratory Groningen, Vol. 40, p. 1
- Owens K. A., Freedman W. L., Madore B. F., Lee A. J., 2022, *ApJ*, 927, 8
- Palladino L. E., Schlesinger K. J., Holley-Bockelmann K., Allende Prieto C., Beers T. C., Lee Y. S., Schneider D. P., 2014, *ApJ*, 780, 7
- Paumard T. et al., 2006, *ApJ*, 643, 1011
- Pecaut M. J., Mamajek E. E., 2013, *ApJS*, 208, 9
- Pejcha O., Thompson T. A., 2015, *ApJ*, 801, 90
- Pelupessy F. I., van Elteren A., de Vries N., McMillan S. L. W., Drost N., Portegies Zwart S. F., 2013, *A&A*, 557, A84
- Perets H. B., Šubr L., 2012, *ApJ*, 751, 133
- Perets H. B., Hopman C., Alexander T., 2007, *ApJ*, 656, 709
- Perley D. A. et al., 2020, *ApJ*, 904, 35
- Pfuhl O. et al., 2011, *ApJ*, 741, 108
- Planck Collaboration VI 2020, *A&A*, 641, A6
- Portegies Zwart S. F., 2000, *ApJ*, 544, 437
- Portegies Zwart S., McMillan S., 2018, *Astrophysical Recipes; The art of AMUSE*. IOP Publishing, Bristol
- Portegies Zwart S. et al., 2009, *New Astron.*, 14, 369
- Portegies Zwart S., McMillan S. L. W., van Elteren E., Pelupessy I., de Vries N., 2013, *Comput. Phys. Commun.*, 184, 456
- Poveda A., Ruiz J., Allen C., 1967, *Bol. Obs. Tonantzintla Tacubaya*, 4, 86
- Rasskazov A., Fragione G., Leigh N. W. C., Tagawa H., Sesana A., Price-Whelan A., Rossi E. M., 2019, *ApJ*, 878, 17
- Renzo M. et al., 2019, *A&A*, 624, A66
- Rich R. M., Ryde N., Thorsbro B., Fritz T. K., Schultheis M., Origlia L., Jönsson H., 2017, *AJ*, 154, 239
- Riello M. et al., 2021, *A&A*, 649, A3
- Rossi E. M., Kobayashi S., Sari R., 2014, *ApJ*, 795, 125
- Rossi E. M., Marchetti T., Cacciato M., Kuiack M., Sari R., 2017, *MNRAS*, 467, 1844
- Rozwadowska K., Vissani F., Cappellaro E., 2021, *New Astron.*, 83, 101498
- Salpeter E. E., 1955, *ApJ*, 121, 161 (S55)
- Sana H. et al., 2012, *Science*, 337, 444
- Sana H. et al., 2013, *A&A*, 550, A107
- Sari R., Kobayashi S., Rossi E. M., 2010, *ApJ*, 708, 605
- Schödel R., Feldmeier A., Neumayer N., Meyer L., Yelda S., 2014a, *Class. Quantum Gravity*, 31, 244007
- Schödel R., Feldmeier A., Kunneriath D., Stolovy S., Neumayer N., Amaro-Seoane P., Nishiyama S., 2014b, *A&A*, 566, A47
- Schödel R., Nogueras-Lara F., Gallego-Cano E., Shahzamanian B., Gallego-Calvente A. T., Gardini A., 2020, *A&A*, 641, A102
- Sesana A., Haardt F., Madau P., 2006, *ApJ*, 651, 392
- Sesana A., Haardt F., Madau P., 2007, *MNRAS*, 379, L45
- Shappee B. J. et al., 2014, *ApJ*, 788, 48
- Shen K. J. et al., 2018, *ApJ*, 865, 15
- Steinmetz M. et al., 2006, *AJ*, 132, 1645
- Stone N. C., Vasiliev E., Kesden M., Rossi E. M., Perets H. B., Amaro-Seoane P., 2020, *Space Sci. Rev.*, 216, 35
- Sukhbold T., Adams S., 2020, *MNRAS*, 492, 2578
- Sukhbold T., Ertl T., Woosley S. E., Brown J. M., Janka H. T., 2016, *ApJ*, 821, 38
- Sukhbold T., Woosley S. E., Heger A., 2018, *ApJ*, 860, 93
- Tauris T. M., 2015, *MNRAS*, 448, L6
- Tauris T. M., Takens R. J., 1998, *A&A*, 330, 1047
- Tillich A., Przybilla N., Scholz R.-D., Heber U., 2009, *A&A*, 507, L37
- Tokovinin A., 2000, *A&A*, 360, 997

- Tonry J. L. et al., 2018, *PASP*, 130, 064505
van Maanen A., 1917, *PASP*, 29, 258
von Fellenberg S. D. et al., 2022, *ApJ*, 932, L6
Wang J., Merritt D., 2004, *ApJ*, 600, 149
Yanny B. et al., 2009, *AJ*, 137, 4377
York D. G. et al., 2000, *AJ*, 120, 1579
Yu Q., Madau P., 2007, *MNRAS*, 379, 1293
Yu Q., Tremaine S., 2003, *ApJ*, 599, 1129
Zhang F., Lu Y., Yu Q., 2013, *ApJ*, 768, 153
- Zhao G., Zhao Y.-H., Chu Y.-Q., Jing Y.-P., Deng L.-C., 2012, *Res. Astron. Astrophys.*, 12, 723
Zheng X., Lin D. N. C., Mao S., 2021, *ApJ*, 914, 33
Zhong J. et al., 2014, *ApJ*, 789, L2
Zubovas K., Wynn G. A., Gualandris A., 2013, *ApJ*, 771, 118

This paper has been typeset from a $\text{\TeX}/\text{\LaTeX}$ file prepared by the author.